

## Gold–Telluride–Palladium Mineralization, a New Type of Mineralization in Gabbro–Dolerites of the Pai-Khoi Ridge (Yugor Peninsula, Russia)

R.I. Shaybekov<sup>a, ✉</sup>, N.V. Sokerina<sup>a</sup>, S.I. Isaenko<sup>a</sup>, N.N. Zykin<sup>b</sup>, S.N. Shanina<sup>a</sup>

<sup>a</sup> Yushkin Institute of Geology, Komi Science Center, Ural Branch of the Russian Academy of Sciences, ul. Pervomaiskaja 54, Syktyvkar, 167982, Russia

<sup>b</sup> LLC Gazprom VNIIGAZ, Proektiruemyi proezd 5537 15/1, s.p. Razvilkovskoe, Leninsky dist., Moscow region, 142717, Russia

Received 30 January 2018; received in revised form 30 July 2019; accepted 28 November 2019

**Abstract**—Data on gabbro-dolerite pyrite–chalcopyrite–pyrrhotite, quartz vein sphalerite–chalcopyrite, and associated early and late gold–telluride–palladium mineralization of the Krutoi ore occurrence (Pai-Khoi Ridge, Yugor Peninsula) are presented. The early (magmatic) gold–telluride–palladium mineralization is represented by minerals of the ternary system Ag–Au–Cu, palladium antimonides and stibiotellurides, and platinum arsenides, and the late (hydrothermal) one, by minerals of the binary systems Au–Ag and Au–Pd as well as mercury, lead, and silver tellurides. Sudburyite and testibiopalladite have been first found in the Krutoi ore occurrence; moreover, testibiopalladite has been first discovered in the Pai-Khoi Ridge. Their chemical compositions and Raman spectra have been examined. The results of sulfide sulfur, oxygen, and carbon isotope studies of calcium-containing minerals of chalcopyrite–quartz veinlets suggest assimilation of the material of the host deposits by the ore-forming mantle fluids. The fluid inclusions in the veinlets are divided into nitrogen–methane and carbon dioxide–nitrogen according to the composition of the gas phase. It has been established that the mineral-forming fluids were poorly saturated with gas. Magnesium and calcium salts were predominant in them. The temperature of the formation of quartz in the chalcopyrite–quartz veinlets is close to 300–490 °C, and sphalerite–chalcopyrite and associated late gold–telluride–palladium mineralization formed at temperatures not exceeding 260 °C.

**Keywords:** Gabbro-dolerite, Krutoi ore occurrence, Pai-Khoi Ridge, chalcopyrite–quartz veinlets, gold–telluride–palladium mineralization, fluid inclusions, gas chromatography, Raman spectroscopy

### INTRODUCTION

Sulfide mineralization spatially and genetically associated with gabbro-dolerite sills and dikes has been long known within the Yugor Peninsula located in the far northeast of European Russia, in the Arkhangelsk Region, between the Barents Sea and the Kara Sea (Ustritskii, 1954). However, the first geological survey on a scale of 1:50,000 in this area was performed by Sopchinskaya and Nyalpeiskaya Geological Prospecting & Survey Teams (GPSTs) in 1966–1970. The geologic structure and composition of intrusive rocks are described in detail elsewhere (Zaborin, 1975; Ostashchenko, 1979; Chernyshov et al., 1990). The first information about the presence of precious metals in gabbro-dolerites of the Pai-Khoi Ridge was provided by Yu.V. Zhukov. Later, N.M. Chernyshov presented results of Pt and Pd analyses of 10 samples from the Savabei, Severnyi, Ruchei, Khengur-1, Pervyi, and Zaozernyi ore occurrences (Chernyshov et al., 1990). The repeated investigation of the mineralized zones at the Krutoi site, performed by CJSC Polyargeo in the framework of the GDP-200 project, yielded Au =

0.11–0.43 and Pd = 0.03–0.10 ppm. These contents of precious metals do not give an idea of their mineral species. The report by Yu.V. Zhukov and his colleagues provides only information about sulfide mineralization and the bulk contents of some chalcogenides in gabbro-dolerites. Earlier we studied sulfide and precious-metal mineralization in quartz veinlets cutting gabbro-dolerites in the Krutoi ore occurrence (Shaybekov, 2013a; Sokerina et al., 2016). However, our data did not give complete information about the distribution of these types of mineralization, their formation conditions, the mineral composition, and the presence of precious metals in the gabbro-dolerites. Therefore, we carried out a comprehensive research into the ore mineralization in gabbro-dolerites of the axial part of the sill and in the cutting thin quartz veins within the Krutoi ore occurrence. The goal of the research was to determine the paragenetic sequence of mineral formation, to elucidate the distribution of precious-metal and sulfide minerals, and to make their typification.

### THE OBJECT OF STUDY

The Krutoi ore occurrence (68°53'N, 63°54'E) is located in the southwest of the Krutoi site, on the right bank of the

✉ Corresponding author.

E-mail address: shaybekov@geo.komisc.ru (R.I. Shaybekov)

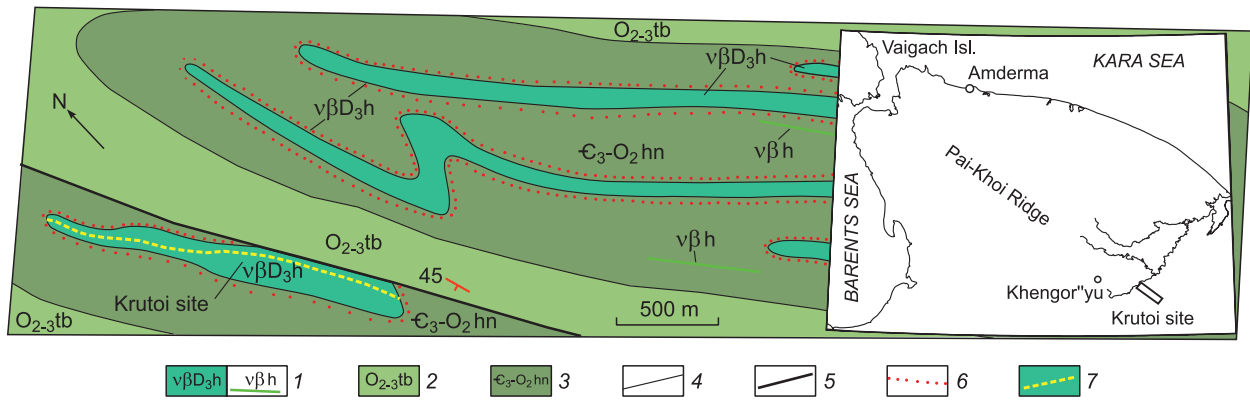


**Fig. 1.** Geological map of the Krutoi site. 1, Khengur (Central Pai-Khoi) gabbro-dolerite complex: gabbro-dolerites, picrodolerites, and dolerites; 2, Tal'beityvis Formation: calcareous sandstones, siltstones, sandy limestones, siliceous-argillaceous shales, and, in places, basalts and tuffaceous lavas; 3, Khengur Formation: argillaceous-siliceous and siliceous-argillaceous shales, their carboniferous varieties, limestones, and, in places, basalts, tuffaceous lavas, sandstones, siltstones, gritstones, conglomerates, silty shales, and carbonaceous-argillaceous shales; 4, geologic boundaries; 5, faults; 6, contact hornfelses; 7, predicted zone of gold–telluride–palladium mineralization.

Khengor'yu River in its upper course, 500 m southeast of the mouth of the Krutoi Brook. It is an elongate conformable sheet gabbro-dolerite body of NW strike ( $v\beta D_3h$ , Fig. 1), dipping at 60–70° and localized among terrigenous-sedimentary rocks of the Khengur Formation ( $C_3-O_2hn$ ). By now, the gabbro-dolerites, like the Khengur complex as a whole, have been dated at the Late Devonian–early Carboniferous (Podsosov, 2000). The recently obtained U–Pb zircon dates show that the above sheet intrusions are of Late Devonian age (Shaybekov, 2006; Shishkin et al., 2009).

The intrusive body hosting ore mineralization has a distinct zonal structure: dolerite porphyrites at the endocontact with the host rocks, light greenish-gray fine-grained glomerogranular dolerites on the periphery, and coarse- and medium-grained prismatic amphibolized quartz gabbro-dolerites in the central part. The body has a number of pinches

and swells along the strike; its visible thickness is within 60–200 m.

The pinches and swells include a zone of regular 1–2 mm dissemination of pyrite–chalcopyrite–pyrrhotite mineralization (5–20%; on average, 7–10%). The zone is several tens of cm to 20 m in visible thickness. It was traced by trenches for 1.5 km at 80–120 m intervals (Fig. 2). The predominant pyrrhotite and subordinate ( $\leq 1\%$ ) chalcopyrite and pyrite occur as worm-like veinlets, grain intergrowths, inclusions, and compact clusters in assemblage with quartz–albite myrmekite. They also fill the interstices between chaotically localized prismatic plagioclase grains, sometimes forming discontinuous rims at their edge. The intrusive body is cut by numerous thin (5–10 cm) chalcopyrite–quartz veinlets.

Despite their metamorphism, gabbro-dolerites hosting ore mineralization have preserved their relict structure. They

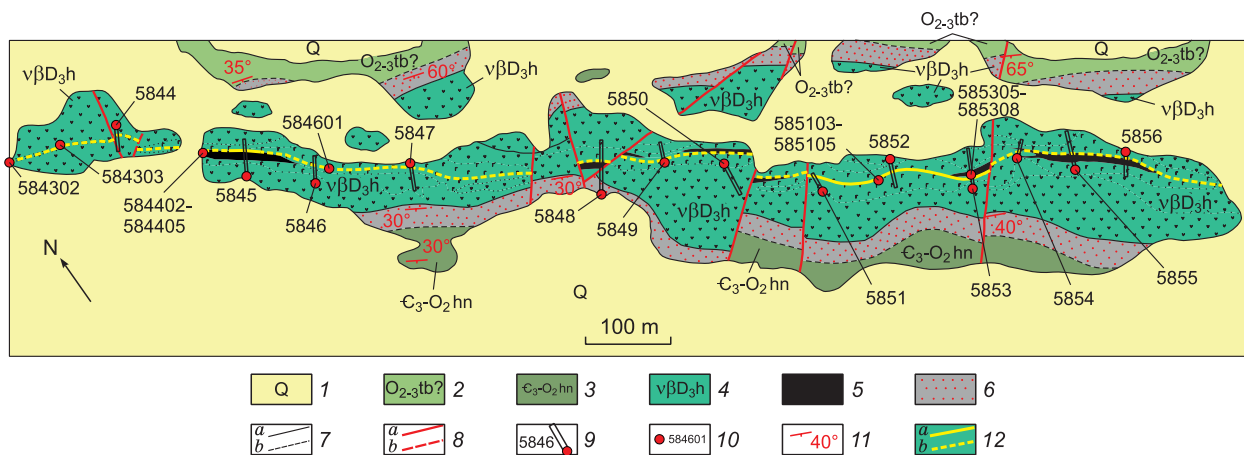


**Fig. 2.** Geological map of the Krutoi site, compiled by O.V. Zaborin (Zhukov et al., 1969), modified and supplemented. 1, Quaternary deposits; 2, Tal'beityvis Formation ( $O_{2-3tb}$ ). Dark gray thin-platy argillaceous shales; 3, Khengur Formation ( $C_3-O_2hn$ ). Light gray platy quartz–albite schists; 4, Khengur gabbro-dolerite complex ( $v\beta D_3h$ ). Gabbro-dolerites: melanocratic coarse-grained quartz, mesoleucocratic medium-grained porphyritic quartz-containing, and glomerogranular; 5, zone of disseminated pyrite–chalcopyrite–pyrrhotite mineralization ( $>10\%$ ); 6, zone of contact hornfelses; 7, geologic boundaries: *a*, proved, *b*, predicted; 8, faults: *a*, proved, *b*, predicted; 9, trenches and their numbers, red circles are our observation/sampling points; 10, sample numbers; 11, rock dip; 12, zone of gold–telluride–palladium mineralization: *a*, proved, *b*, predicted.

**Table 1.** Chemical composition of rocks, wt.%

Component	Contents of components		
	584401 (melanocratic coarse-grained gabbro-dolerite, Krutoi ore occurrence)	585308 (melanocratic coarse-grained quartz-containing gabbro-dolerite, Krutoi ore occurrence)	Average chemical composition (108 analyses) of rocks of the Khengur complex (Shaybekov, 2013)
SiO <sub>2</sub>	49.20	51.21	49.04
TiO <sub>2</sub>	1.99	2.21	1.44
Al <sub>2</sub> O <sub>3</sub>	15.10	15.19	13.55
Fe <sub>2</sub> O <sub>3</sub>	4.55	2.95	3.12
MnO	0.18	0.19	0.19
MgO	5.50	4.65	7.19
CaO	7.63	6.72	10.15
Na <sub>2</sub> O	2.54	3.56	2.20
K <sub>2</sub> O	0.24	0.53	0.63
P <sub>2</sub> O <sub>5</sub>	—	—	0.09
LOI	4.22	3.89	4.01
Total	100.00	100.00	100.00
Fe <sub>2</sub> O <sub>3tot</sub>	14.39	12.83	13.46
FeO	8.86	8.90	8.41
H <sub>2</sub> O	0.40	0.49	0.37

Note. Hereafter, dash — not found. The chemical composition of rocks was determined by X-ray fluorescence spectroscopy on an XRF-1800 Shimadzu spectrometer (analyst S.T. Neverov). The H<sub>2</sub>O and FeO contents and LOI were determined by a quantitative chemical analysis, and the Na<sub>2</sub>O and K<sub>2</sub>O contents were measured on an FP-640 flame photometer.

consist of partly or highly saussuritized plagioclase, variably altered clinopyroxene (overgrown with brown hornblende), quartz, quartz–albite myrmekite, and accessory minerals (apatite, ilmenite, titanite, pyrrhotite, rutile, zircon, etc.). In the chemical composition the rocks of the Krutoi ore occurrence are generally identical to the rocks of the Khengur gabbro-dolerite complex (Table 1).

According to earlier data (chemical analysis of furrow samples), the contents of mineral-forming components in the gabbro-dolerites were as follows (%): Cu = 0.01–0.1, Ni = 0.001–0.01, and Co = 0.007–0.01. Recent chemical analysis of furrow, ore lump, and shearing samples of gabbro-dolerites and quartz–sulfide veinlets has shown a Cu content of 0.09–0.67% and Ni and Co contents below their fire assay–AAS detection limits.

The petrochemical composition of these gabbro-dolerites and the host rocks is described in more detail by Silaev (1978).

## METHODS

The SEM images of ore mineralization were obtained at the Institute of Geology UB RAS, Syktyvkar, using a TESCAN Vega3 LMH scanning electron microscope with an accelerating voltage of 20 kV and a current of 15 nA (analysts S.S. Shevchuk and E.M. Tropnikov). The chemical analysis of minerals was performed in the EDS mode, using an Oxford Instruments INCA X-MAX (50 mm) X-ray microprobe

with an accelerating voltage of 20 kV, a current of 15 nA, a vacuum of 0.05 Pa, and a beam diameter of 2 μm. Exposure time, 500 000 pulses Standards and characteristic lines: Pt (Pt L<sub>α</sub>), Pd (Pd L<sub>α</sub>), Au (Au M<sub>α</sub>), Ag (Ag L<sub>α</sub>), Pb, Te (Pb Te, Pb M<sub>α</sub>, Te L<sub>α</sub>), Bi (Bi M<sub>α</sub>), Sb (Sb L<sub>α</sub>), Cu (Cu K<sub>α</sub>), Ni (Ni K<sub>α</sub>), Fe, S (FeS<sub>2</sub>, Fe K<sub>α</sub>, S K<sub>α</sub>), Hg (HgTe, Hg M<sub>α</sub>), Co (Co K<sub>α</sub>), Zn (Zn K<sub>α</sub>, L<sub>α</sub>), As (InAs, As L<sub>α</sub>), Se (Se L<sub>α</sub>), Cd (Cd L<sub>α</sub>), Ti (Ti K<sub>α</sub>), V (V K<sub>α</sub>), Mn (Mn K<sub>α</sub>), Ca (wollastonite K<sub>α</sub>), Si, O (SiO<sub>2</sub>, Si K<sub>α</sub>), Al (Al<sub>2</sub>O<sub>3</sub>, Al K<sub>α</sub>), K (KBr K<sub>α</sub>), Mg (MgO K<sub>α</sub>), Sc (Sc K<sub>α</sub>), Na (albite K<sub>α</sub>), U (U M<sub>α</sub>), Th (ThO<sub>2</sub> M<sub>α</sub>), P (P K<sub>α</sub>), and Sn (Sn L<sub>α</sub>). The detection limits of ore-forming elements (>3σ criterion) (wt.%): Se, Cd, and Ni — 0.1–0.2, S, Fe, Zn, Cu, Pb, Sb, Hg, Te, Co, Sn, Pd, As, Bi, and Ag — 0.2–0.4, Pt — 0.5, Mo — 0.6, and Au — 0.4–0.8.

Monomineral fractions were separated and sampled from chalcopyrite–quartz veinlets as follows. The 300 g samples were crushed to the fraction 0.25–0.50 mm, sieved, treated with bromoform to separate the light fraction, and separated into magnetic and nonmagnetic parts using a Sochnev magnet. Then, the obtained concentrates of the light, magnetic, and nonmagnetic fractions were cleaned manually under a binocular microscope (analysts N.K. Khachatryan and R.I. Shaybekov, Syktyvkar) to separate monofractions of ore and nonmetallic minerals. First, the separated monofractions were placed on a conductive double-sided carbon tape and were subjected to carbon spraying for a subsequent SEM study of the natural surfaces and cavities. Then, the same mineral grains were placed in an epoxy washer for surface polishing permitting a study of their internal compo-

sition. In addition, samples with chalcopyrite grains were taken for isotope analysis of sulfur, and quartz–albite–epidote aggregates were sampled for measuring the isotopic composition of carbon and oxygen.

Analysis for precious metals was carried out in the Central Laboratory of A.P. Karpinsky Russian Geological Research Institute, St. Petersburg (analysts V.A. Shishlov and V.L. Kudryashov), following technique 17 based on Russian Federation Patent No. 2425363 “A method for measuring the contents of precious metals in rocks and mining dumps” dated 27 July 2011 (the patent priority date is 17 May 2010). The technique consists in chemical decomposition of samples with a complex of concentrated acids, fusion of the residue with sodium peroxide, dissolution of the alloy in HCl, and ICP MS analysis of the solution on an Agilent 7700x mass spectrometer ensuring an efficient removal of isobaric noise during a PGE analysis. This technique ensures a detection limit of 0.002 ppm for all PGE.

The structure of minerals was determined by X-ray diffraction analysis (Shimadzu XRD-6000 diffractometer, Cu anode, current of 30 mA, voltage of 30 kV, Ni filter, 2 $\theta$  scanning step of 0.05°, recording speed of 1 g/min) (analysts Yu.S. Simakova and B.A. Makeev, Syktyvkar). The maximum permissible error in the measurement of 2 $\theta$  was  $\pm 0.025^\circ$ .

Isotope analysis of sulfur in chalcopyrite from chalcopyrite–quartz veinlets was carried out on a Finnigan MAT 253 (ThermoFinnigan, Bremen, Germany) mass spectrometer in the Laboratory of Stable Isotopes of the Center for Common Use of the Far Eastern Geological Institute, Vladivostok (analyst T.A. Velivetskaya), following the technique of a dual injection system elaborated by Grinenko (1962). The sulfur isotope composition is given relative to the CDT standard (sulfur of troilite from the Canyon-Diablo meteorite). The mass of the analyzed samples was 10 mg. The error in the determination of  $\delta^{34}\text{S}$  ( $2\sigma$ ) was  $\pm 0.1\%$ .

Carbonates were decomposed in  $\text{H}_3\text{PO}_4$  for mass spectrometry studies. The isotopic compositions of carbon and oxygen in calcites were measured (analyst I.V. Smoleva, Syktyvkar) by flow mass spectrometry in a helium flow (CF-IRMS), using a ThermoFisher Scientific (Bremen, Germany) analytical setup including a GasBench II gas preparation and introduction system connected to a DELTA V Advantage mass spectrometer. The  $\delta^{13}\text{C}$  values are given relative to the PDB standard, and the  $\delta^{18}\text{O}$  values, relative to the SMOW standard. The NBS 18 and NBS 19 international standards were also used during the measurements. The error in the measurement of  $\delta^{13}\text{C}$  and  $\delta^{18}\text{O}$  was  $\pm 0.1\%$ .

Fluid inclusions in quartz were studied in polished plates using a Linkam THMSG600 heating/freezing stage, which permits measurements at temperatures from  $-196$  to  $600^\circ\text{C}$ . The measurement error was  $<1^\circ\text{C}$ . The salinity of the inclusion fluids was evaluated from the melting point of ice. The salt composition of the inclusions was determined from the eutectic temperature of the water–salt system (Borisenko, 1977). The syngenetic nature of the inclusions was estab-

lished from their arrangement. Syngenetic inclusions included primary and primary–secondary inclusions localized singly, in small groups, or in quartz cracks.

For identification of minerals and gases in the inclusions, Raman spectra of the polished plates were recorded on a LabRam HR 800 (Horiba Jobin Yvon) spectrometer at room temperature at the Geonauka Common Use Center of the Institute of Geology, Syktyvkar. The spectrum recording conditions: monochromator grating, 600 l/mm; confocal aperture, 300 and 500  $\mu\text{m}$ ; slit, 100  $\mu\text{m}$ ; exposure time, 1–10 s; number of signal accumulation cycles, 10; exciting-radiation power of a He–Ne laser ( $\lambda = 632.8\text{ nm}$ ), 20 mW; and exciting-radiation power of an Ar<sup>+</sup> laser, 12 mW ( $\lambda = 514.5\text{ nm}$ ). After registering the Raman spectra of the samples, the positions of the maxima of the spectral lines were determined by the convolution of the Gauss–Lorentz functions of the LabSpec standard spectrum processing program (5.36).

The bulk composition of the inclusion gases was analyzed with a Tsvet 800 gas chromatograph with an attachment for thermal unsealing of inclusions (analyst S.N. Shanina, Syktyvkar). The analysis was carried out using 0.5 g quartz samples (fractions 0.25–0.50 mm). The inclusions were unsealed at 500, 600, 800 and 1000  $^\circ\text{C}$ . The samples were heated in the reactor in the helium atmosphere. The detection limit for the main components was as follows ( $\mu\text{L}$ ):  $2 \times 10^{-2}$  for  $\text{N}_2$  and  $\text{CO}$ ,  $3 \times 10^{-2}$  for  $\text{CH}_4$  and  $\text{CO}_2$ , and  $3 \times 10^{-3}$  for  $\text{H}_2\text{O}$  (Borisenko, 1977).

## RESULTS

**Mineralogical and geochemical characteristics.** The ore zone is nonuniformly distributed within the intrusive body and is localized mostly in melanocratic quartz and quartz-containing coarse-grained gabbro-dolerites. This fact is established by field observations and results of analysis of the small number of furrow (dash-furrow) and lump ore samples (Shaybekov, 2013a).

Comprehensive studies of the ore zone revealed pyrite–chalcopyrite–pyrrhotite and sphalerite–chalcopyrite quartz vein mineralization spatially and genetically associated with gold–telluride–palladium mineralization.

*Sphalerite–chalcopyrite quartz vein mineralization* has been first found by us in the Krutoi ore occurrence. It is localized in thin chalcopyrite–quartz veinlets.

Analysis of the mineral composition of chalcopyrite–quartz veinlets has shown that quartz prevails ( $>98\%$ ), sphalerite and chalcopyrite add up to 1%, and quartz–albite–epidote aggregates amount to  $<1\%$ .

*Quartz* is the main mineral in the quartz veinlets. It occurs as transparent milky-white grains of different sizes intergrown with chalcopyrite and quartz–albite–epidote aggregates. The grains are often covered with iron hydroxides.

*Quartz–albite–epidote aggregates* were identified in a binocular study of the heavy-fraction minerals. These are

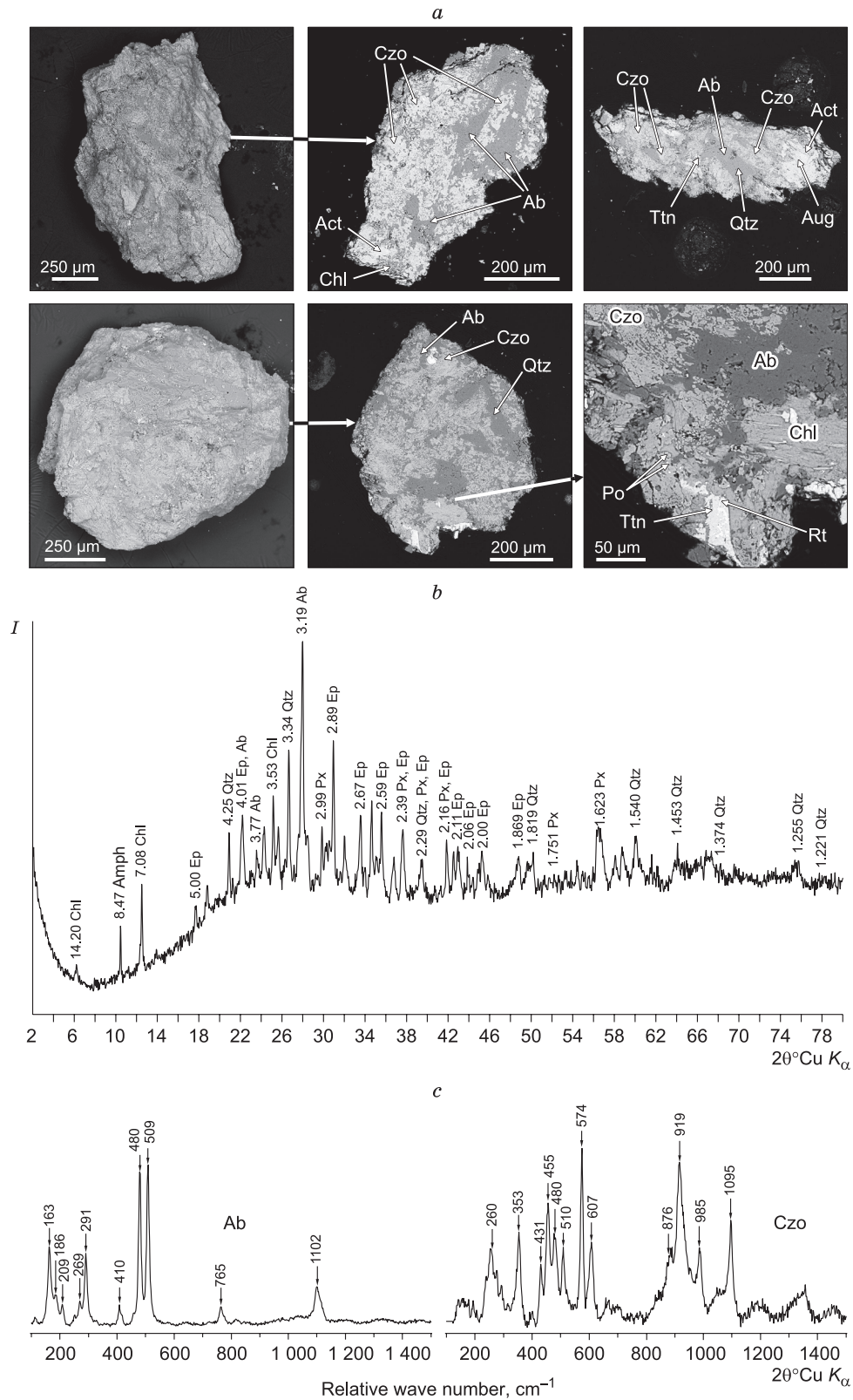


**Fig. 3.** Quartz–albite–epidote aggregate. *a*, BSE images: on the left is natural surface, on the right is polished surface; *b*, diffraction pattern of aggregate; *c*, diffraction patterns of albite and clinozoisite. Czo, clinozoisite; Ab, albite; Aug, augite; Chl, chlorite; Act, actinolite; Qtz, quartz; Ttn, titanite; Po, pyrrhotite; Rt, rutile; Ep, epidote; Amph, amphibole; Px, pyroxene.

**Table 2.** Chemical composition of minerals of quartz–albite–epidote aggregate, wt.%

Na <sub>2</sub> O	MgO	Al <sub>2</sub> O <sub>3</sub>	SiO <sub>2</sub>	K <sub>2</sub> O	CaO	Sc <sub>2</sub> O <sub>3</sub>	TiO <sub>2</sub>	V <sub>2</sub> O <sub>5</sub>	MnO	FeO	Σ
Epidote (clinozoisite)											
—	—	30.71	40.80	—	22.29	—	—	—	—	3.99	97.79
2.95	—	29.49	46.06	—	17.93	—	—	—	—	2.37	98.80
—	—	31.30	39.79	—	24.21	—	—	—	—	4.77	100.07
—	—	30.69	40.23	—	24.55	—	—	—	—	4.42	99.89
—	—	32.74	39.63	—	24.68	—	—	—	—	2.26	99.31
—	—	32.55	39.95	—	24.61	—	—	—	—	2.15	99.26
—	—	31.55	40.15	—	24.22	0.33	—	—	—	3.70	99.95
Plagioclase (albite)											
11.13	—	20.07	68.80	—	0.37	—	—	—	—	—	100.37
11.26	—	20.08	68.18	0.13	0.53	—	—	—	—	—	100.18
11.25	—	19.94	69.13	—	—	—	—	—	—	—	100.32
11.26	—	20.03	69.12	—	—	—	—	—	—	—	100.41
11.08	—	20.04	68.59	—	0.33	—	—	—	—	—	100.03
11.01	—	20.51	68.82	—	—	—	—	—	—	—	100.34
Chlorite											
—	17.32	20.13	27.90	—	—	—	—	—	0.27	22.91	88.54
—	16.55	19.80	29.24	—	0.15	—	—	—	0.33	21.84	87.91
Amphibole (actinolite)											
—	15.21	1.70	54.68	—	12.13	0.19	—	—	0.25	14.59	98.75
—	16.28	1.37	56.12	—	13.07	0.19	—	—	0.16	12.20	99.39
Pyroxene (augite)											
—	13.15	1.58	52.06	—	21.92	—	—	—	—	11.10	99.81
Titanite											
—	—	1.7	30.71	—	28.34	—	39.02	—	—	0.46	100.23
Rutile											
—	—	—	—	—	—	—	99.93	1.09	—	—	101.02
Quartz											
—	—	—	100.23	—	—	—	—	—	—	—	100.23

Note. The chemical compositions of clinozoisite, actinolite, and chlorite are given without water.

light green to gray sugar-like nonrounded angular grains measuring fractions to few millimeters. Electron microscope study showed that the aggregates are compact intergrowths of quartz, albite, augite, clinozoisite, and chlorite (Fig. 3a). The ratio of the intensities of basalt reflexes and  $hkl = 0.60$  with  $d/n \sim 1.497 \text{ \AA}$  in the X-ray diffraction patterns of the aggregates (Fig. 3b) suggest the presence of dioctahedral mica (muscovite). Raman spectroscopy confirmed that albite and clinozoisite are the main minerals of the aggregates (Fig. 3c). The chemical composition of the minerals of the quartz–albite–epidote aggregate is given in Table 2.

*Chalcopyrite* is another main mineral in the quartz veinlets. It occurs mostly as nests, schlieren up to 2 cm in size, and, more seldom, fine (1–4 mm) dissemination and veinlets in quartz (Fig. 4a). It has a highly cracked surface and voids

filled with quartz (Fig. 4c). The chemical composition of chalcopyrite ( $n = 15$ ) is variable (wt.%; the parenthesized value is the average content): Cu = 24.82–33.86 (32.84), Fe = 28.56–34.92 (30.99), and S = 33.96–39.18 (35.54); the total is 99.31–100.88 (99.84). One sample contains impurities of Ni (3.97) and Ag (2.96) (Table 3). The Cu/Fe ratio varies from 0.71 to 1.11, averaging 1.06. Thus, the mineral has a deficit of Cu, whereas Fe and S are often present in excess. The calculated average empirical formula of the chalcopyrite is  $\text{Cu}_{0.95}\text{Fe}_{1.02}\text{S}_{2.03}$ .

There are iron hydroxides and covellite with Ag inclusions on the periphery and in the cracks of chalcopyrite (Fig. 4a, d; Tables 3 and 4). In addition, sphalerite with impurities of Cd, Fe, and Cu (most likely, trapped during the matrix analysis), cassiterite, gold, porpezite, empressite,

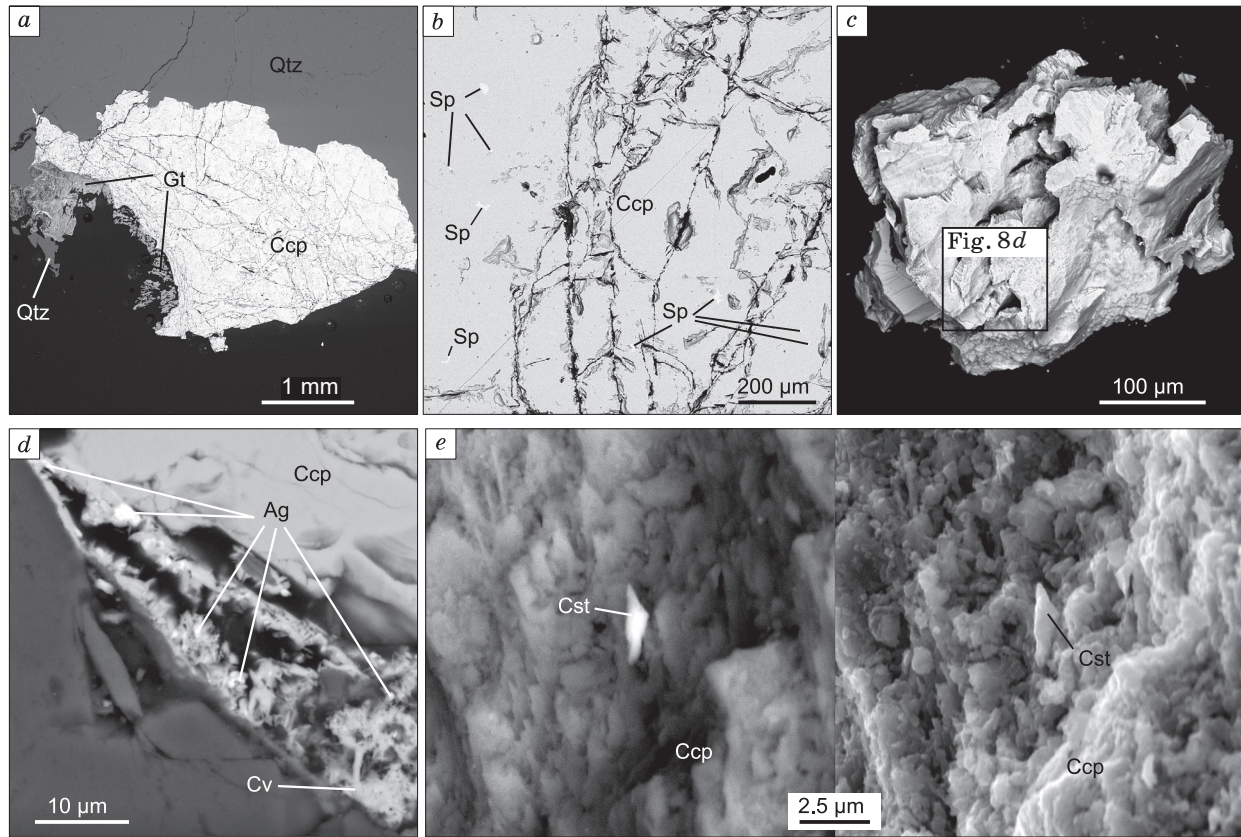


**Fig. 4.** Ore mineralization of quartz–sulfide veinlets (BSE images). *a*, Chalcopyrite intergrown with quartz, polished surface; *b*, chalcopyrite with spherulite inclusions; *c*, grain, natural surface; *d*, chalcopyrite with covellite rim containing silver inclusions; *e*, chalcopyrite intergrown with cassiterite (on the right, SE image of the natural surface). Qtz, quartz; Gt, hydrogoethite; Ccp, chalcopyrite; Sp, spherulite; Ag, silver; Cv, covellite; Cst, cassiterite.

hessite, altaite, and coloradoite are present as inclusions and intergrowths (Fig. 4*b*; Table 3).

*Iron hydroxides (hydrogoethite)* are found in hypergenetic zones and are the product of oxidation of sulfide minerals. Their segregations measure few millimeters, have a colloform concentric zonal structure, and usually form rims over chalcopyrite grains with pyrrhotite and spherulite inclusions (Fig. 5*a–c*). These iron hydroxides ( $n = 23$ , Table 4) have the following chemical composition (wt.%):  $\text{Fe}_2\text{O}_3 = 65.74\text{--}76.81$  (73.67),  $\text{CuO} = 1.81\text{--}2.49$  (2.04),  $\text{SO}_3 = 2.72\text{--}5.72$  (4.26),  $\text{SiO}_2 = 0.56\text{--}2.03$  (1.04),  $\text{Al}_2\text{O}_3$  ( $n = 5$ ) =  $0.17\text{--}0.28$  (0.21),  $\text{P}_2\text{O}_5$  ( $n = 4$ ) =  $0.23\text{--}0.39$  (0.29),  $\text{K}_2\text{O}$  ( $n = 1$ ) = 0.19, and  $\text{CaO}$  ( $n = 1$ ) = 0.15; the total (without  $\text{H}_2\text{O}$ ) is  $72.66\text{--}84.48$  (81.12). Since it is impossible to establish the mineral type of iron hydroxides from their chemical composition, we examined them by Raman spectroscopy (Fig. 5). The spectra have three narrow peaks at **217**, **287**, and **396**  $\text{cm}^{-1}$ . These wavenumbers are typical of goethite (Oh et al., 1998), which is characterized by the following wavenumbers ( $\text{cm}^{-1}$ ) (the parenthesized values are data from other authors mentioned in the above paper; the wavenumbers of intense peaks are bold-typed): 205, 247 (245), **300 (303)**, **386 (390, 397)**, 418 (420), 481 (480, 485), and 549 (550, 554).

*Pyrite–chalcopyrite–pyrrhotite mineralization.* This type of mineralization is specific to gabbro–dolerites in the axial zone of the intrusive body. *Pyrrhotite* is its most abundant ore mineral. It has xenomorphous cavernous cracked grains of irregular shape, few microns to few centimeters in size, localized among rock-forming minerals. Pyrrhotite is present in assemblage with apatite, ilmenite, titanite, K-feldspars, pyrite, chalcopyrite, and quartz (Fig. 6, Tables 5 and 6). It has a stable chemical composition with a slight deficit of iron and excess sulfur (Table 5,  $n = 14$ , wt.%):  $\text{Fe} = 59.62\text{--}60.76$  (60.09),  $\text{S} = 39.06\text{--}40.20$  (39.50), the total is  $99.04\text{--}100.29$  (99.60). The calculated empirical formula of the pyrrhotite is  $\text{Fe}_{0.93}\text{S}_{1.00}$ . The mineral contains inclusions of *sphalerite* (free of Cd impurities in contrast to sphalerite present in chalcopyrite of quartz–sulfide veinlets), *hessite*, and *altaite*. Native *lead* and *galena* with Se and Te impurities are often found in its cracks. One sample contains an intergrowth of pyrrhotite and *cubanite* (Fig. 6*c*).

*Chalcopyrite* is scarcer and occurs as phenocrysts in silicates and as rims over pyrrhotite grains. Often, chalcopyrite, together with pyrrhotite, forms nests and is localized in their cores. Chalcopyrite is also present as intergrowths with galena containing an impurity of Se. The chalcopyrite segrega-

tions measure few tens of microns to several millimeters. The chemical composition of the mineral shows minor variations (Table 5,  $n = 6$ , wt.%): Cu = 32.26–33.78 (33.30), Fe = 29.85–32.64 (30.68), S = 34.40–35.73 (35.11), the total is 98.09–100.88 (99.22); one sample contains an impurity of Zn. The Cu/Fe ratio varies from 1.06 to 1.11, averaging 1.09. Chalcopyrite of this mineral assemblage has a more stable composition than chalcopyrite of sphalerite–chalcopyrite assemblage, which has a deficit of Cu.

The identified Ti minerals are, most likely, the exsolution product of titanomagnetite, namely, titanite and ilmenite (Table 6). Ilmenite occurs mainly as elongate drop-like grains forming myrmekite structures and, less often, as large skeletal segregations intensely replaced by titanite and overgrown with hornblende, often chloritized. These segregations measure few microns to 7–10 mm and are in assemblage with sulfides present as xenomorphic grains in ilmenite interstices, which suggests the later genesis of sulfides. Single ilmenite segregations contain bornite inclusions few tens of microns in size.

In addition, we have found an intergrowth of *cobaltite* (Co = 32.24, Ni = 2.40, As = 45.79, and S = 19.20; the total is 100.03 wt.%) and sphalerite in ilmenite, a *molybdenite* inclusion in hornblende (Mo = 58.15, S = 41.37, the total is 99.52 wt.%), and native *bismuth* and *cassiterite* in the interstices of rock-forming minerals.

*Gold–telluride–palladium mineralization.* This type of mineralization has been first revealed in the Pai-Khoi Ridge and can be subdivided into early and late assemblages according to its composition and spatial occurrence.

Early magmatic mineral assemblage (minerals of the ternary Ag–Au–Cu system, sudburyite, and sperrylite) is present only together with pyrite–chalcopyrite–pyrrhotite mineralization in the axial zone of the gabbro–dolerite sill. An ICP MS analysis of three gabbro–dolerite samples from this zone showed the following contents of PGE (ppm): Ru < 0.0020, Rh ≤ 0.0110, Pd ≤ 0.0470, Ir ≤ 0.0070, Pt ≤ 0.0190, and Au ≤ 0.0057. The early assemblage of gold–telluride–palladium mineralization of the Krutoi ore occurrence is usually nonuniformly disseminated in pyrrhotite, hornblende, albite, and chlorite; in the latter minerals it always coexists with sulfides.

*Minerals of the Ag–Au–Cu system* of this assemblage are mostly the products of exsolution of Ag–Au–Cu phases. Their isometric grains are ≤ 5 μm in size (mainly, few microns) and are localized as inclusions in the rock-forming minerals and pyrrhotite (Fig. 7a, f). The above ternary system significantly varies in composition because of Cu and Ag impurities. We have not revealed a dependence of this composition on the size and localization of inclusions, which might be due to a small number of the studied samples. Only two samples are similar in chemical composition to *cuproauride* (AuCu<sub>3</sub>) and *tetra-auricupride* (AuCu); the rest are varieties of *Cu-containing gold* or *Au-containing copper* (Table 7). These Ag–Au–Cu minerals were recognized approximately, because they differ in syngony and the

**Table 3.** Chemical composition of sulfide minerals, wt.%

Cu	Fe	S	Zn	Cd	Ag	Σ
<b>Chalcopyrite</b>						
24.82	34.92	33.96	—	—	2.96	100.63*
31.59	28.56	39.18	—	—	—	99.33
32.96	30.82	35.58	—	—	—	99.36
33.78	30.75	35.16	—	—	—	99.69
33.78	31.36	35.73	—	—	—	100.88
33.86	31.07	35.48	—	—	—	100.42
33.56	31.03	35.39	—	—	—	99.98
33.55	30.91	35.17	—	—	—	99.63
33.40	30.39	35.72	—	—	—	99.51
33.77	30.92	35.35	—	—	—	100.04
33.43	30.87	35.18	—	—	—	99.49
33.45	30.85	35.21	—	—	—	99.51
33.57	30.48	35.48	—	—	—	99.53
33.38	30.63	35.30	—	—	—	99.31
33.72	31.35	35.14	—	—	—	100.22
<b>Sphalerite</b>						
1.64	7.46	33.12	56.02	1.96	—	100.21
—	7.90	33.94	56.67	1.88	—	100.38
—	10.28	33.29	55.40	1.90	—	100.87
3.10	8.33	33.42	52.31	2.06	—	99.21
1.22	7.82	33.43	55.42	1.97	—	99.85
1.29	7.55	33.41	55.37	1.71	—	99.33
<b>Covellite</b>						
52.29	11.58	36.43	—	—	0.53	100.83
60.01	1.55	34.03	—	—	3.66	99.25
57.28	7.48	35.63	—	—	0.37	100.76

\* Ni = 3.97.

sizes of microinclusions of Cu-containing gold make it impossible to obtain structural data.

Platinum minerals are represented by occasional isometric *sperrylite* (PtAs<sub>2</sub>) grains few microns in size in albite (Fig. 7d). The mineral has the following chemical composition ( $n = 2$ , wt.%): Pt = 54.93 and 55.65 (55.29), As = 43.06 and 43.36 (43.21), and Fe = 0.30 and 0.67 (0.49); the total is 98.59 and 99.37 (98.98). The calculated empirical formula is Pt<sub>0.91</sub>As<sub>2.09</sub>. There are also scarce grains of *sudburyite* (PdSb) and *testibiopalladite* (Pd(Sb,Bi)Te) up to 5 μm in size in chlorite and amphibole (Fig. 7e, f). A mineral compositionally similar to sudburyite was first found in the mineralization zone of Mt. Khengor’yu (Shaybekov, 2018). Testibiopalladite has been first revealed in the Pai-Khoi Ridge. Figure 7g presents the Raman spectra of these minerals. The spectrum of sudburyite has peaks at wavenumbers of 83, 114, 174, 286, and 461 cm<sup>-1</sup>, and the spectrum of *testibiopalladite*, at 81, 96, **113**, 127, **142**, and 155 cm<sup>-1</sup> (the intense peaks are bold-typed). There are many research works concerned with Raman spectroscopy of Pd tellurides. The most

**Table 4.** Chemical composition of iron hydroxides (hydrogoethite), wt.%

Al <sub>2</sub> O <sub>3</sub>	SiO <sub>2</sub>	P <sub>2</sub> O <sub>5</sub>	SO <sub>3</sub>	K <sub>2</sub> O	CaO	Fe <sub>2</sub> O <sub>3</sub>	CuO	H <sub>2</sub> O*	Σ (without H <sub>2</sub> O)
0.25	1.22	—	4.40	—	—	74.03	2.49	17.61	82.39
0.17	1.75	—	2.74	—	0.15	65.74	2.10	27.34	72.66
—	1.81	0.27	3.40	—	—	72.02	1.99	20.51	79.49
—	1.05	—	2.72	—	—	72.21	1.82	22.20	77.80
—	2.03	—	3.20	—	—	71.44	1.85	21.48	78.52
—	0.70	0.23	4.41	—	—	72.31	2.11	20.24	79.76
—	0.83	—	5.63	—	—	73.46	2.01	18.08	81.92
0.19	1.30	—	3.38	—	—	72.89	1.88	20.37	79.63
—	0.94	—	3.84	—	—	72.51	1.97	20.74	79.26
—	0.65	—	4.12	—	—	72.46	2.14	20.63	79.37
—	0.79	—	4.97	—	—	74.87	2.01	17.35	82.65
—	0.56	—	5.08	—	—	76.13	1.97	16.26	83.74
0.22	0.95	0.28	3.83	—	—	76.07	2.04	16.60	83.40
—	0.68	—	5.72	—	—	75.63	1.93	16.04	83.96
—	0.66	—	5.44	0.19	—	73.70	2.46	17.55	82.45
—	0.69	—	5.48	—	—	74.90	2.24	16.69	83.31
—	0.68	—	3.68	—	—	76.81	2.03	16.80	83.20
0.20	0.92	0.39	4.18	—	—	76.74	2.05	15.52	84.48
—	0.74	—	4.06	—	—	73.94	1.99	19.28	80.72
—	0.77	—	4.68	—	—	76.79	1.94	15.82	84.18
—	1.74	—	3.64	—	—	73.56	1.91	19.15	80.85
—	1.84	—	4.52	—	—	74.77	1.81	17.06	82.94
—	0.70	—	4.80	—	—	71.51	2.08	20.91	79.09

\* Calculated values.

detailed ones are referenced by Bakker et al. (2014), but this publication lacks Raman spectra of sudburyite and testibiopalladite or spectra similar to those in Fig. 7g. The Raman spectrum of stibiopalladite most similar in composition to testibiopalladite has two characteristic peaks at 108 and 136 cm<sup>-1</sup> and weak peaks at 169 and 187 cm<sup>-1</sup>.

Late hydrothermal mineral assemblage (minerals of the binary Au–Ag and Au–Pd systems and Hg, Pb, and Ag tellurides) is localized in chalcopyrite–quartz veinlets cutting gabbro-dolerites and, partly, in gabbro-dolerites of the axial zone of the sill. Analysis of chalcopyrite from these veinlets showed the following contents of precious metals (ppm): Ru = 0.031, Rh = 0.021, Pd = 0.100, Ir = 0.031, Pt = 0.140, and Au = 0.420; the total content is 0.740.

*Minerals of the Au–Ag and Au–Pd systems* are present as intergrowths of Pd-containing gold (porpezite) and chalcopyrite and as inclusions of native gold in chalcopyrite (Fig. 8b–f, Table 7) of quartz veinlets and in hornblende of gabbro-dolerites in the axial zone of the sill (Fig. 7f, Table 7). The inclusions are mostly 2 to 10 μm (seldom, up to 100 μm) in size. Gold is of medium to high fineness (Petrovskaya, 1993).

*Coloradoite* (HgTe) was first found in the Krutoi ore occurrence in 2013. It is the only finding of this mineral on the

**Table 5.** Chemical composition of sulfide minerals in gabbro-dolerites, wt.%

Cu	Fe	S	Pb	Te	Se	Zn	Σ
<b>Pyrrhotite</b>							
—	60.27	39.06	—	—	—	—	99.33
—	60.11	39.42	—	—	—	—	99.53
—	59.82	39.67	—	—	—	—	99.49
—	60.55	39.74	—	—	—	—	100.29
—	59.77	39.37	—	—	—	—	99.14
—	60.09	39.74	—	—	—	—	99.83
—	59.62	39.42	—	—	—	—	99.04
—	60.27	39.17	—	—	—	—	99.44
—	60.76	39.22	—	—	—	—	99.98
—	60.76	39.38	—	—	—	—	100.14
—	59.88	40.20	—	—	—	—	100.08
—	59.87	39.45	—	—	—	—	99.33
—	59.58	39.57	—	—	—	—	99.15
—	59.94	39.62	—	—	—	—	99.56
<b>Chalcopyrite</b>							
33.78	31.36	35.73	—	—	—	—	100.88
32.77	30.87	34.82	—	—	—	—	98.45
33.11	30.96	34.83	—	—	—	—	98.90
33.78	30.75	35.16	—	—	—	—	99.69
33.11	30.30	34.68	—	—	—	—	98.09
33.24	29.85	35.45	—	—	—	0.74	99.29
<b>Sphalerite</b>							
—	13.83	34.85	—	—	—	51.66	100.35
—	7.60	31.74	—	—	—	60.53	99.88
<b>Pyrite</b>							
—	47.36	52.73	—	—	—	—	100.09
—	47.22	53.54	—	—	—	—	100.76
<b>Galena</b>							
—	—	13.63	84.61	—	—	—	98.24
0.90	1.94	11.13	82.78	—	3.46	—	100.21
—	0.92	11.53	86.39	—	0.79	—	99.62
<b>Bornite</b>							
62.014	12.28	25.91	—	—	—	—	100.20
<b>Cubanite</b>							
24.33	40.50	35.05	—	—	—	—	99.88
<b>Native lead</b>							
—	—	—	88.16	0.61	8.59	—	100.37
—	—	—	99.86	—	—	—	99.86
—	—	—	92.04	—	8.22	—	100.20
—	—	—	96.28	—	1.78	—	98.06

Yugor Peninsula and, in particular, in the Khengur gabbro-dolerite complex (Shaybekov, 2013a). Coloradoite is in intimate assemblage with chalcopyrite in quartz veinlets. It occurs as isometric inclusions several microns in size in chalcopyrite zones subjected to hypergene processes (Fig. 8a) and contains impurities of Ni, Pb, and Ag (Table 7). The

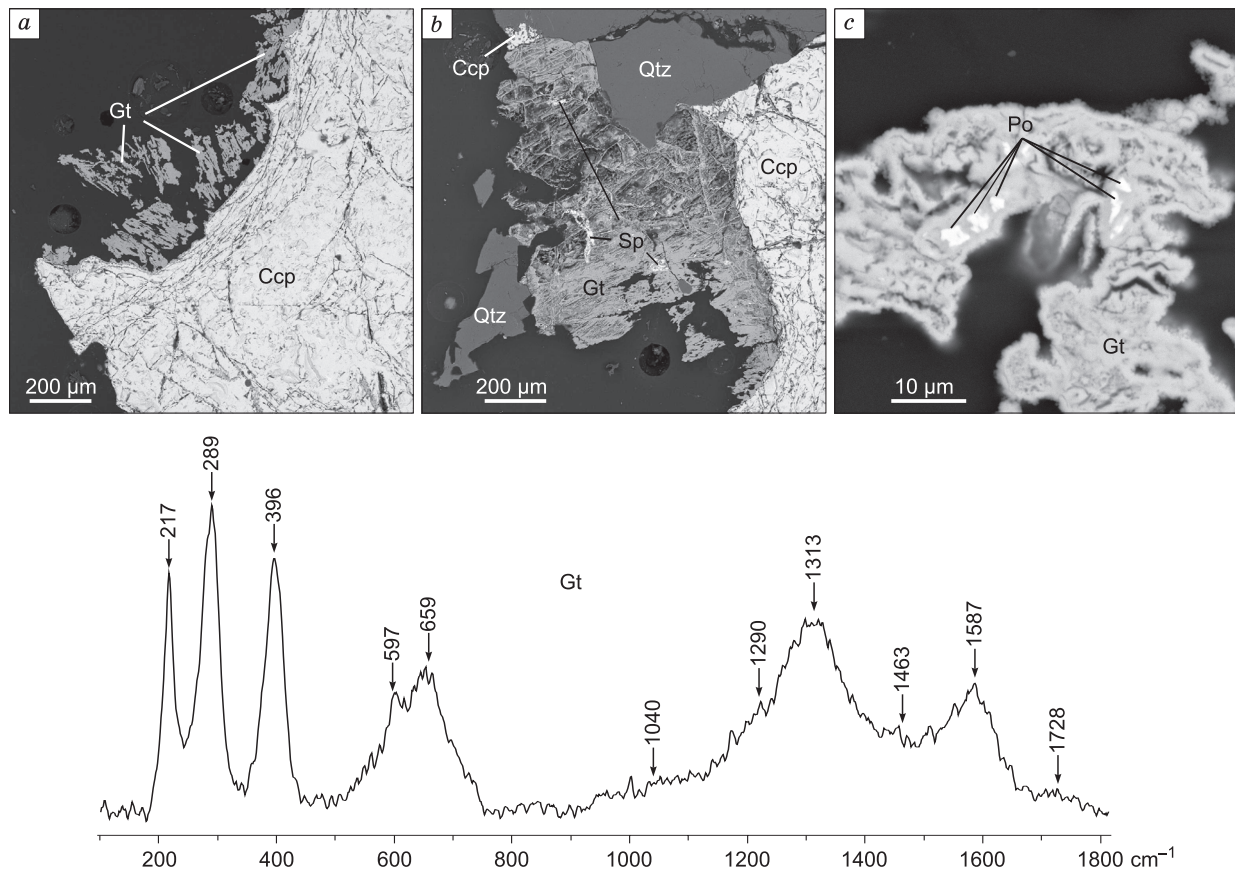


**Fig. 5.** BSE images of iron hydroxides. *a, b*, Iron hydroxide rim with pyrrhotite and sphalerite inclusions; *c*, segregations in pyrrhotite. Below is the Raman spectrum of hydrogoethite.

Ag- and Pb-rich inclusions are, most likely, a mixture of several mineral phases: empressite ( $\text{AgTe}$ ), hessite ( $\text{Ag}_2\text{Te}$ ), altaite ( $\text{PbTe}$ ), and coloradoite ( $\text{HgTe}$ ).

Pyrrhotite in gabbro-dolerites of the axial zone of the sill and chalcopyrite in quartz veinlets contain microinclusions of *altaite* ( $\text{PbTe}$ ), *hessite* ( $\text{Ag}_2\text{Te}$ ), and *empressite* ( $\text{AgTe}$ ). Altaite and hessite in pyrrhotite are individual microinclusions up to  $5\ \mu\text{m}$  in size (Fig. 7*b, c*). Microinclusions in chalcopyrite are usually a fine mixture of altaite and empressite; their small size ( $1\text{--}2\ \mu\text{m}$ ) makes it impossible to determine the exact proportion of the components.

A similar gold–telluride assemblage (porpezite, gold, altaite, hessite, coloradoite, and empressite) is typical of many epithermal gold–telluride deposits of the world (Kovalenker et al., 1990; Cooke and Phail, 2001; Pals and Spry, 2003; Shackleton et al., 2003; Ciobanu et al., 2004; Spry and Scherbarth, 2006; Voudoris, 2006; Nikolaev et al., 2013; Zhai and Liu, 2014).

Chalcopyrite–quartz veinlets with productive late gold–telluride–palladium mineral assemblage were additionally studied.

**The isotopic composition of sulfur, carbon, and oxygen of chalcopyrite–quartz veinlets.** Sulfur of the studied chalcopyrites is characterized by  $\delta^{34}\text{S} = -2.4$  to  $-2.5\text{‰}$  (CDT), which is close to the isotopic composition of sulfur

of igneous rocks formed from mantle sources ( $\delta^{34}\text{S} = -1.5$  до  $+1.5\text{‰}$ ) (Ohmoto and Rye, 1979; Faure, 1986). The slight enrichment of chalcopyrites in light isotope ( $^{32}\text{S}$ ) relative to “mantle” sulfur indicates that the igneous rocks are contaminated with sulfur of sulfides of sedimentary rocks (Ohmoto and Rye, 1979). The isotopic composition of sulfur of chalcopyrite monofractions ( $n = 5$ ) is well persistent, which testifies to a single homogeneous source of sulfur.

The isotopic composition of carbon and oxygen of vein calcite also points to a significant contribution of crustal material to the composition of ore-forming fluids. Oxygen of calcite from a quartz–albite–epidote aggregate ( $n = 5$ ) is characterized by  $\delta^{18}\text{O} = +15.3\text{‰}$  (SMOW), which significantly exceeds the values typical of unaltered igneous rocks ( $\delta^{18}\text{O} = +7\text{‰}$ ) (Taylor, 1974). Calculation shows that  $\text{CO}_2$  being in equilibrium with  $\text{H}_2\text{O}$  in the ore-forming fluid is characterized by  $\delta^{18}\text{O} = 25\text{--}30\text{‰}$  (SMOW) at the fluid homogenization temperatures and formed, most likely, during the thermal dissociation of the host carbonates. The isotopic composition of calcite carbon,  $\delta^{13}\text{C} = -17.7\text{‰}$  (PDB), also indicates the contribution of the material of the host sedimentary rocks. This composition is typical of carbon of carbonates formed during magmatic and hydrothermal processes involving crustal organic matter.

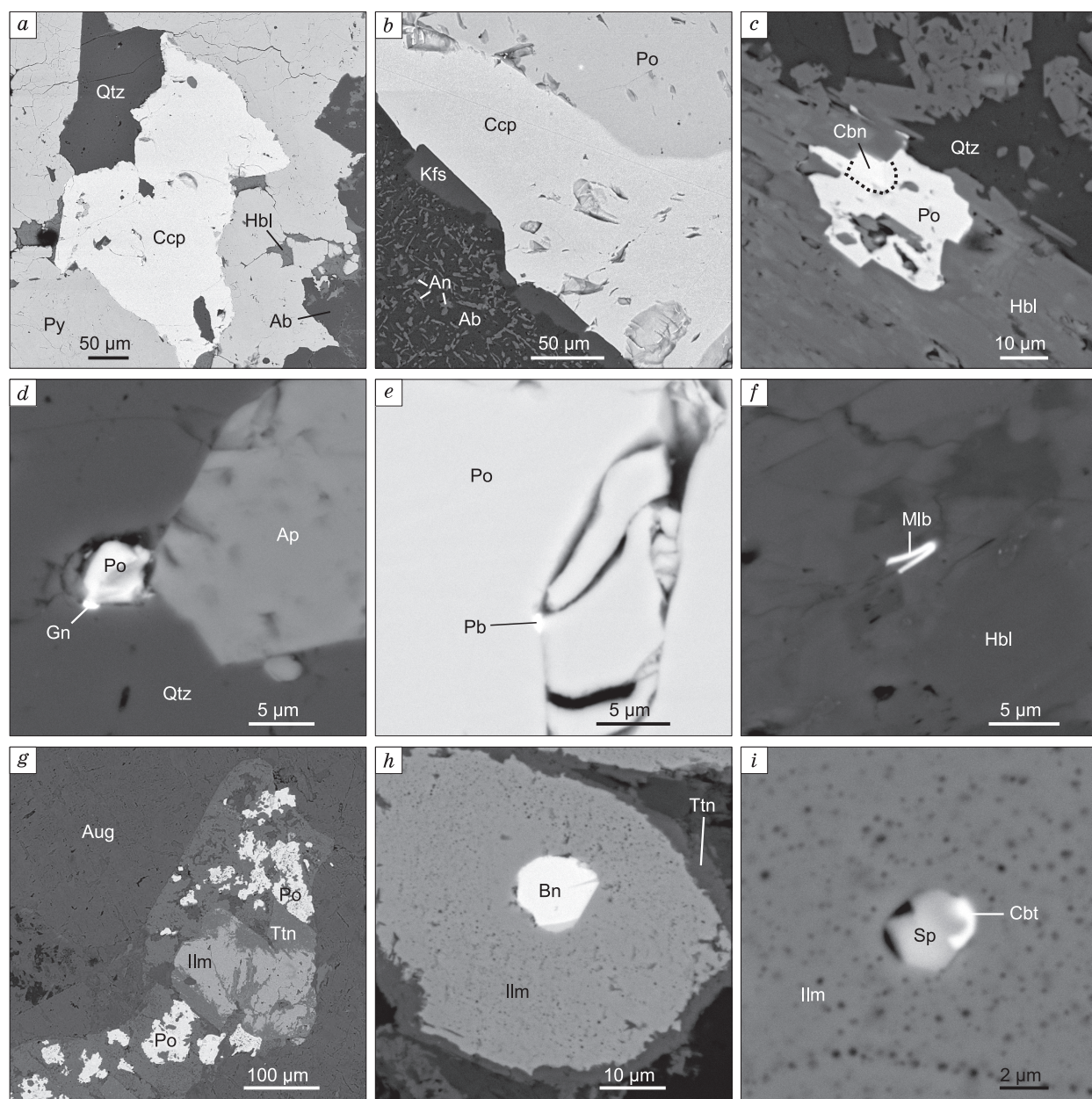


**Fig. 6.** BSE images of ore and accessory mineralization in gabbro-dolerites. Qtz, quartz; Ccp, chalcopyrite; Hbl, hornblende; Ab, albite; Py, pyrite; Po, pyrrhotite; Gn, galena; Ap, apatite; Kfs, K-feldspar; An, anorthite; Aug, augite; Ilm, ilmenite; Ttn, titanite; Sp, sphalerite; Cbt, cobaltite; Mlb, molybdenite; Cbn, cubanite; Pb, native lead; Bn, bornite.

**Study of fluid inclusions in quartz of chalcopyrite–quartz veinlets.** To elucidate the formation conditions of vein quartz and associated ore mineralization, we studied syngenetic (localized singly, in small groups, or in the mineral cracks) fluid inclusions in this quartz. Sometimes, such inclusions are distributed throughout the mineral grain. Special attention was given to inclusions in sulfide (mostly chalcopyrite) zones.

The gas composition of some inclusions was studied by Raman spectroscopy. We have recognized nitrogen–methane and carbon dioxide–nitrogen inclusions. This suggests

two sources of gases, which might be of mantle, crustal, or mixed nature. The origin of gases in inclusions was discussed elsewhere (Mazzini et al., 2011; Sokerina et al., 2013; Smirnov et al., 2014; Zykin and Sokerina, 2015).

Study of the bulk composition of fluid inclusions by gas chromatography showed that the rocks contain little gas (Sokerina et al., 2016) and the inclusions contain mainly water (~99%), which agrees with visual observations. Carbon dioxide is predominant among the gas components, and methane and nitrogen are subordinate. Moreover, on standard heating of quartz to 500 °C, nitrogen was not detected.

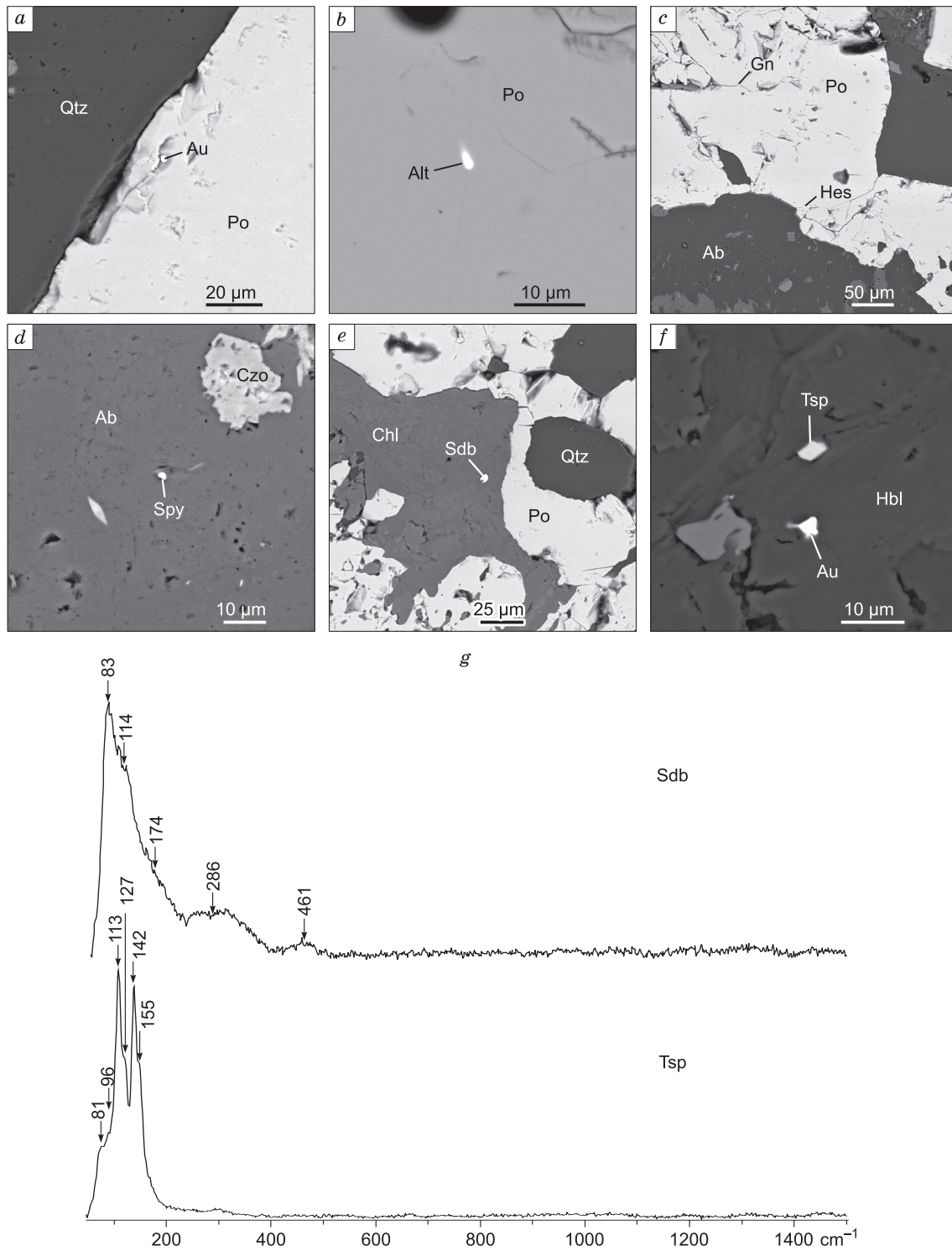


**Fig. 7.** BSE images of early gold–telluride–palladium mineral assemblage. *a–c*, Inclusions in pyrrhotite: *a*, gold, *b*, altaite; *d–f*, inclusions in the interstices of rock-forming minerals: *d*, sperrylite, *e*, Au-containing sudburyite of early assemblage, *f*, gold and testibiopalladite; *g*, Raman spectra (notch filter = 83–85  $\text{cm}^{-1}$ ) of sudburyite and testibiopalladite. Au, gold; Alt, altaite; Gn, galena; Hes, hessite; Ab, albite; Spy, sperrylite; Sdb, sudburyite; Tsp, testibiopalladite; Chl, chlorite; Qtz, quartz; Po, pyrrhotite; Hbl, hornblende; Czo, clinozoicite.

The release of nitrogen and most of methane begins at  $>500$  °C and continues to 800 °C. Taking into account that these gases were reliably established in the inclusions by

Raman spectroscopy, we think they are part of fluid inclusions but not the product of decomposition of organic matter during the sample heating.

**Table 6.** Chemical composition of Ti-containing minerals in gabbro-dolerites, wt.%

TiO <sub>2</sub>	V <sub>2</sub> O <sub>5</sub>	MnO	FeO	CaO	SiO <sub>2</sub>	Al <sub>2</sub> O <sub>3</sub>	Σ
Titanite							
39.17	0.35	—	2.20	27.69	30.32	—	99.73
36.70	2.36	—	1.26	28.54	31.37	—	100.23
38.74	0.61	—	2.28	27.56	30.24	—	99.43
36.39	1.25	—	2.27	27.22	31.04	1.94	100.11
39.02	—	—	0.46	28.34	30.71	1.70	100.23
38.97	—	—	1.39	28.17	29.81	0.69	99.03
38.30	—	—	1.24	26.24	32.56	2.40	100.75
40.79	—	—	—	28.61	31.67	—	101.08
Ilmenite							
52.49	0.63	3.75	43.61	—	—	—	100.49
51.92	0.69	3.61	43.27	—	—	—	99.50
52.72	1.51	3.72	42.64	—	—	—	100.59
53.10	—	3.76	43.62	—	—	—	100.48
52.34	1.43	3.52	42.34	—	—	—	99.63
50.98	2.48	3.16	42.94	—	—	—	99.56
53.87	—	3.98	42.82	—	—	—	100.68

**Table 7.** Chemical composition of minerals of gold–telluride–palladium mineralization, wt.%

Au	Ag	Pd	Cu	Ni	Pb	Te	Sb	Hg	Σ	Note
Early assemblage										
58.44	10.16	—	30.68	—	—	—	—	—	99.28	Au <sub>0.68</sub> Ag <sub>0.22</sub> Cu <sub>1.11</sub>
68.79	10.21	—	21.46	—	—	—	—	—	100.46	Au <sub>0.89</sub> Ag <sub>0.24</sub> Cu <sub>0.86</sub>
85.43	—	—	14.19	—	—	—	—	—	99.62	Cu <sub>1.36</sub> Au <sub>1.64</sub>
61.67	2.78	—	35.71	—	—	—	—	—	100.17	Au <sub>0.35</sub> Ag <sub>0.03</sub> Cu <sub>0.62</sub>
72.07	—	—	27.92	—	—	—	—	—	99.99	AuCu (Au <sub>0.91</sub> Cu <sub>1.09</sub> )
33.13	2.69	—	64.68	—	—	—	—	—	100.50	Au <sub>0.14</sub> Ag <sub>0.02</sub> Cu <sub>0.84</sub>
35.50	2.77	—	61.30	—	—	—	—	—	99.56	Au <sub>0.15</sub> Ag <sub>0.02</sub> Cu <sub>0.82</sub>
—	—	44.54	—	—	—	4.10	51.14	—	99.84	Pd <sub>0.97</sub> (Sb <sub>0.96</sub> Te <sub>0.07</sub> ) <sub>1.03</sub>
—	—	27.69	—	—	—	32.28	26.14	—	99.62	(Pd <sub>0.95</sub> Fe <sub>0.13</sub> ) <sub>1.08</sub> Te <sub>0.93</sub> (Sb <sub>0.79</sub> Bi <sub>0.20</sub> ) <sub>0.99</sub> (Fe = 2.04, Bi = 11.33)
Late assemblage										
94.83	—	5.10	—	—	—	—	—	—	99.93	Pzt (Pd <sub>0.09</sub> Au <sub>0.91</sub> )
96.14	—	3.66	—	—	—	—	—	—	99.80	Pzt (Pd <sub>0.07</sub> Au <sub>0.93</sub> )
85.02	15.30	—	—	—	—	—	—	—	100.32	Au (847 ‰)
92.01	7.43	—	—	—	—	—	—	—	99.50	Au (925 ‰)
100.80	—	—	—	—	—	—	—	—	100.80	Au
99.99	—	—	—	—	—	—	—	—	99.99	Au
92.55	7.26	—	—	—	—	—	—	—	99.81	Au (rim, 927 ‰)
98.80	—	—	—	—	—	—	—	—	98.80	Au (core)
—	1.13	—	—	—	—	41.02	—	57.60	99.76	Clr ((Hg <sub>0.93</sub> Ag <sub>0.03</sub> ) <sub>0.96</sub> Te <sub>1.04</sub> )
—	47.82	—	—	—	8.07	31.13	—	13.92	100.94	Mix (Clr+Alt+Em)
—	1.77	—	—	0.54	4.72	37.74	—	55.10	99.87	Clr ((Hg <sub>0.89</sub> Pb <sub>0.07</sub> Ag <sub>0.05</sub> Ni <sub>0.03</sub> ) <sub>1.04</sub> Te <sub>0.96</sub> )
—	5.22	—	—	1.59	13.88	31.42	—	45.87	97.97	Mix (Clr+Alt+Em)
—	19.46	—	—	—	—	33.23	—	46.67	99.36	Mix (Clr+Em)
—	62.73	—	—	—	—	36.71	—	—	99.44	Hes
—	—	—	—	—	62.94	36.67	—	—	99.61	Alt

Note. Au, gold, AuCu, tetra-auricupride, Pzt, porpezite, Clr, coloradoite, Alt, altaite, Em, empressite.

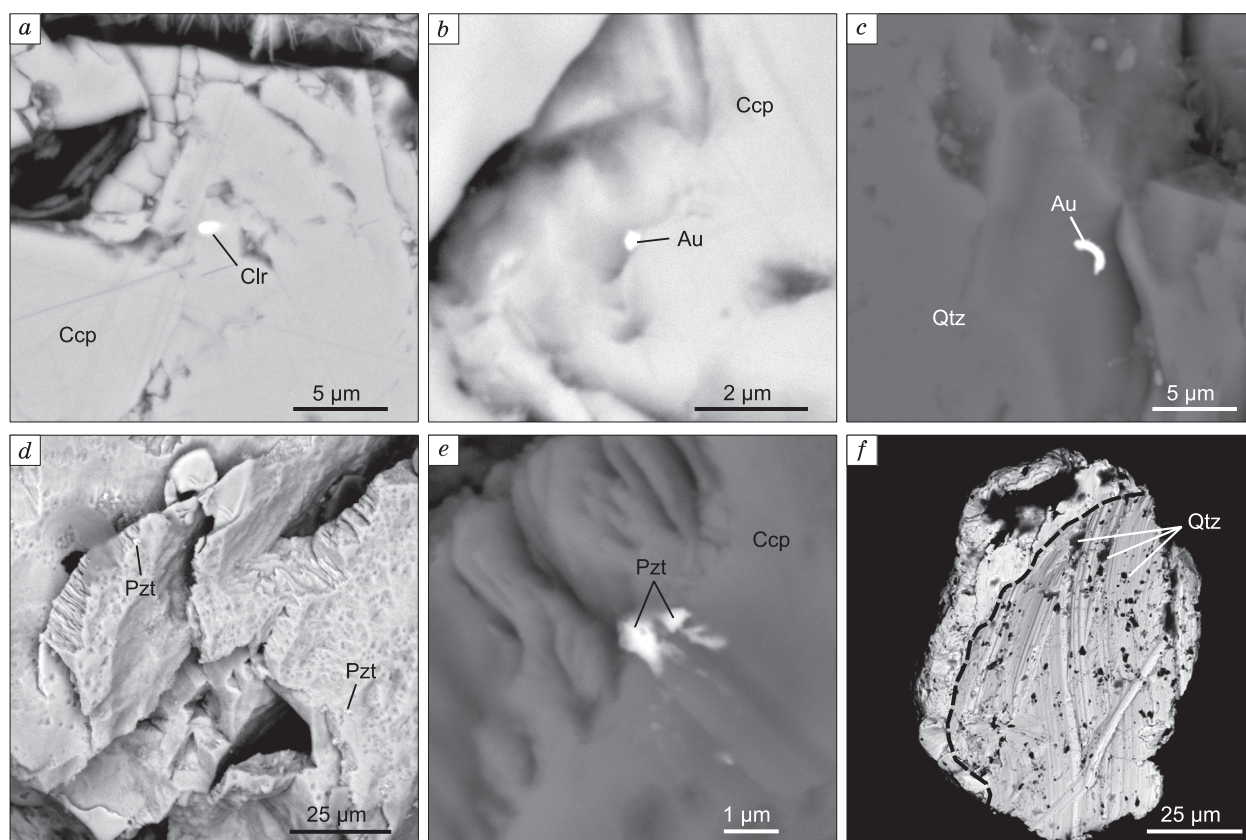


**Fig. 8.** BSE images of late gold–telluride–palladium mineral assemblage. *a*, Coloradoite in chalcopyrite; *b*, gold in chalcopyrite; *c*, gold in quartz; *d*, intergrowths of porpezite and chalcopyrite; *e*, intergrowth of porpezite and chalcopyrite; *f*, gold grain with a high-fineness core and Ag-containing rim. *a–c*, *e*, *f*, polished surface; *d*, natural surface. Ccp, chalcopyrite; Clr, coloradoite; Au, gold; Qtz, quartz; Pzt, porpezite.

## DISCUSSION

The early study showed that the precious-metal mineralization in gabbro-dolerites of the Khengur complex is mostly of magmatogene and hydrothermal nature (Shaybekov, 2013b).

The revealed early gold–telluride–palladium mineral assemblage of the Krutoi site comprises Ag–Au–Cu minerals (predominantly Cu-containing gold and Au-containing copper), sperrylite, sudburyite, and testibiopalladite.

The highest-temperature minerals of this assemblage are sudburyite, testibiopalladite, and sperrylite. Sudburyite is the first to crystallize. Its synthetic analogue melts at 800 °C. At 600 °C, it forms a complete isomorphous series with kotulskite PdTe and with nonequilibrium solid solutions with compositions intermediate between PdTe and PdTe<sub>2</sub> produced at 575–710 °C (Kim and Chao, 1991; Barkov et al., 2002; Makovicky, 2002). Some researchers (Dare et al., 2010; Barnes et al., 2016) classify sperrylite as a high-temperature mineral with crystallization temperatures of 900–1200 °C. Others (Hanley 2007; Piña et al., 2012; Helmy et al., 2013; Bai et al., 2017) believe that sperrylite, along with testibiopalladite, can form in magmatic sulfide ores through crystallization from a residual sulfide melt at a low tempera-

ture, which is limited to the lower interval of the melting temperatures of Cu-enriched magmatic sulfide liquid (Craig and Kullerud, 1969).

Copper-containing gold is usually considered in the framework of the binary Au–Cu system including solid solutions and intermetallic compounds (auricupride, cuproauride, tetra-auricupride, and CuAu<sub>3</sub>). Since this gold often contains an impurity of Ag (sometimes, significant), it is more correct to consider the Ag–Au–Cu system. Lozhechkin (1939) showed the phase inhomogeneity of Cu-containing gold as a result of exsolution of the Au–Cu–Ag phase and its platy intergrowth with electrum. Much later, Murzin et al. (1987) established that Cu-containing gold corresponds in composition to the AuCu phase and that electrum has a fineness of 470–610‰. Experimental studies of the ternary system Ag–Au–Cu demonstrated that the solubility of all of its components significantly decreases as the temperature drops from 700 to 350 °C and lower (Chang et al., 1977). The serious temperature decrease significantly restricts the formation of Ag–Au–Cu minerals but does not prevent the formation of the binary Au–Ag and Au–Cu phases with a wide range of compositions (Murzin and Varlamov, 2018). The arrangement of the composition points of Cu-containing gold in the Ag–Au–Cu diagram with iso-

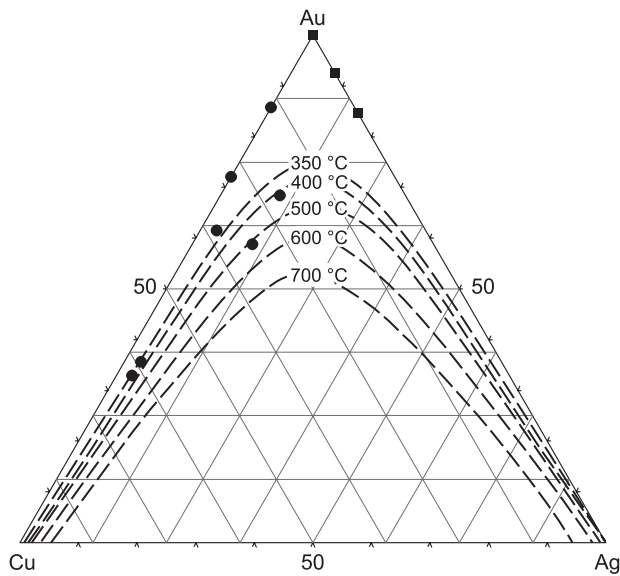


**Fig. 9.** Au–Ag–Cu composition diagram (wt.%) with solid-solution isotherms for gold of early (black circles) and late (black squares) gold–telluride–palladium mineral assemblages, based on experimental data (Murzin and Varlamov, 2018).

therms of ternary solid solutions shows that this gold might have formed at 350–500 °C, whereas the temperatures of formation of cuproauride and tetra-auricupride are somewhat lower (Fig. 9). According to Okamoto et al. (1987), the temperature of the phase transition of CuAu II (35–65 at.% Au, i.e.,  $\text{Cu}_2\text{Au}$ – $\text{CuAu}_2$ , “rozkhovite”) into CuAu I (40–60 at.% Au, i.e.,  $\text{Cu}_3\text{Au}_2$ – $\text{Cu}_2\text{Au}_3$ , tetra-auricupride) is about 385 °C.

The late gold–telluride–palladium mineral assemblage occurs as porpezite intergrowths, as inclusions of native gold and silver, altaite, empressite (hessite), and coloradoite in chalcopyrite of quartz veinlets, and as inclusions of altaite and hessite in pyrrhotite of gabbro-dolerites in the axial zone of the Krutoi ore occurrence.

Afifi et al. (1988a,b) were among the first to summarize available data on the thermodynamics of the phase equilibria of tellurides, including data for ore deposits, obtained in the temperature range 100–300 °C and with variations in  $f_{\text{Te}_2}$ ,  $f_{\text{S}_2}$ , and  $f_{\text{O}_2}$ . As follows from these data, the above mineral assemblage formed with decreasing temperature and  $f_{\text{Te}_2}$  and increasing  $f_{\text{S}_2}$ , which might have been due to the mixing of reduced hydrothermal high-temperature fluids and oxygen-saturated seawater (Cabri, 1965; Afifi et al., 1988a,b; Maslennikov et al., 2013). Some researchers believe that the simultaneous deposition of native gold, native silver, and tellurides (altaite, hessite, coloradoite, and empressite) took place at 150–200 °C (other authors report 130–200 °C for these minerals (Vikentyev, 2006) and 230–260 °C for electrum, altaite, and hessite (Maslennikov et al., 2013)) and at pH ~ 6–8 (Hannington and Scott, 1989; Bortnikov et al., 2003). Earlier experimental data showed that empressite is stable at  $T < 210$  °C (Honea, 1964) (according

to recent data, at  $T < 191$  °C (Voronin et al., 2017)) and the intermediate phase of monoclinic (low-temperature) hessite  $a\text{Ag}_2\text{Te}$  is stable at  $T < 145$  °C (Karakaya and Thompson, 1991).

The study of fluid inclusions in chalcopyrite–quartz veinlets has shown their formation under decrease in temperature from 490–300 to 260–134 °C, which is typical of the formation of gold–quartz–sulfide veins and was earlier established in the Novogodnee-Monto, Petropavlovskoe, Berznyakovskoe, Byn’govskoe, Kochkanarskoe, and other gold deposits in the Urals (Prokof’ev and Spiridonov, 2000; Andreev and Mansurov, 2008; Plotinskaya and Groznova, 2008; Klyukin, 2012; Mansurov, 2013). These deposits bear gold–telluride mineralization. Many researchers report the oxidizing conditions of mineral formation there (Prokof’ev and Spiridonov, 2000; Plotinskaya and Groznova, 2008; Klyukin, 2012), which are evident as a predominance of  $\text{CO}_2$  in the fluid and as the presence of inclusions with high-density carbon dioxide. Under carbon dioxide action, low-grade and dispersed ores transformed into commercial ones (Roizenman, 2008). The Krutoi ore occurrence lacks a zone saturated with  $\text{CO}_2$ -rich fluids. Quartz veins and associated precious-metal mineralization formed under reducing conditions, as evidenced by Raman spectroscopy studies of the composition of fluid inclusions. The mineral-forming fluid was poor in gas. On heating to 500 °C, the fluid amounts to no more than 360 ppm, and most of it is water. The varying salt composition of inclusions, expressed in a wide range of eutectic temperatures, might be due to tremolite ( $\text{Ca}_2\text{Mg}_5(\text{OH})_2[\text{Si}_4\text{O}_{11}]$ ) acicules in quartz. The high salinity suggests the magmatic origin of the mineral-forming solutions. There is a direct correlation between the salinity and the homogenization temperature, which indicates a gradual cooling of the mineral-forming medium.

It is difficult to compare gold–telluride–palladium mineralization of the Krutoi ore occurrence with gold ores of the Urals and Siberia because of the different geologic structures, ages, and compositions of the ore-hosting rocks, different geodynamics, genesis, localization of ore minerals, etc. The Krutoi ore occurrence is most similar in mineral composition to the Ozernoe ore occurrence with an assemblage of precious metals and copper sulfides and with significant contents of Pd and Te impurities and minerals (Kuznetsov et al., 2014). In Siberia, the most similar deposits are located in the Norilsk ore field. They are rich in low-temperature mineral assemblages containing Au, Ag, As, Pd, Pt, Sn, Bi, Sb, and Te (Spiridonov and Gritsenko, 2009). The ICP MS data on chalcopyrite from quartz veinlets and on the host gabbro-dolerites with sulfide mineralization have shown that the veinlets are the main concentrators of precious metals. We have established that Pd is present in the chalcopyrite–quartz veinlets as porpezite, whereas the species of Pt are still debatable. Taking into account that the estimated crystallization temperature of sulfides in the chalcopyrite–quartz veinlets is  $< 260$  °C, we assume that Pt is present as a microimpurity either in sulfides (which is typi-

cal of sulfides of magmatic Cu–Ni deposits (Cabri, 2002; Dare et al., 2010, 2011; Helmi et al., 2013) or in Coloradoite (Augé et al., 2002). Another possible source of Pt is gold and Pd-containing gold, which often contain microimpurities of Pt, not exceeding few hundredths or few tenths of percent, which are not detected in an EDS analysis. We do not rule out the presence of unrecognized inclusions of low-temperature platinum minerals. For example, at 230–240 °C, cooperite (PtS) can be produced from hydrothermal solutions contained in sulfides (Evstigneeva and Tarkian, 1996). Metallic platinum crystallizes in a hydrothermal solution at 200–300 °C, and sperrylite, at  $\leq 300$  °C (Plyusnina et al., 2007; Plyusnina and Likhoidov, 2009). A similar fact is reported by Watkinson and Melling (1992) for sperrylite in assemblage with high-temperature copper sulfides. Platinum minerals are also recognized in hydrothermal low-temperature mineral assemblages of the Norilsk ore field (Spiridonov and Gritsenko, 2009). Although platinum is found as sperrylite in sulfides of gabbro-dolerites in the axial zone of the Krutoi site, its content is negligible (ICP MS data).

## CONCLUSIONS

Based on the results of detailed studies of the ore zone of the Krutoi ore occurrence (Pai-Khoi Ridge), two types of sulfide mineralization have been recognized: pyrite–chalcopyrite–pyrrhotite (in gabbro-dolerites) and sphalerite–chalcopyrite (in quartz veins), which are spatially and genetically associated with gold–telluride–palladium mineralization. The formation of chalcopyrite–quartz veins with gold–telluride–palladium mineralization in the Krutoi ore occurrence is consistent with the concept of the hydrothermal stage of mineral formation. According to this concept, ore components accumulated in the residual fluid at the final stages of hydrothermal process. This fluid participated in the formation of postmagmatic hydrothermal mineralization, as evidenced both by the relationship between chalcopyrite–quartz veinlets and host gabbro-dolerites and by the composition of gas–liquid inclusions.

We have established that the vein quartz formed at 300–490 °C and the sphalerite–chalcopyrite mineralization and associated late gold–telluride–palladium mineralization were produced at  $\leq 260$  °C. The mineral-forming solution contained Mg and Ca salts, whose excess led to the formation of filamentous tremolite crystals in vein quartz. The mineral-forming fluid was poor in gas. The isotopic compositions of sulfur, carbon, and oxygen of the studied minerals formed during magmatic and hydrothermal processes conform to the concepts of contamination of magmatic minerals with sulfur, oxygen, and carbon of the host sedimentary rocks.

Gold–telluride–palladium mineralization in assemblages of different ages has been first revealed in the study area. It is of great interest, because tellurides, bismuthotellurides, and gold and palladium minerals are also present in other ore occurrences and mineralization sites within the Pai-Khoi

gabbro-dolerite complexes. This indicates that the region is promising for precious metals. The recorded Raman spectra of sudburyite and testibiopalladite in gabbro-dolerites of the axial zone of the Krutoi ore occurrence permit one to use Raman spectroscopy as an additional method for identifying these minerals.

This work was carried out in the framework of the state assignment research (grant AAAA-A17-117121270036-7) at the Geoscience Center for Common Use of the Institute of Geology, Syktyvkar, and with partial financial support by basic research grant 15-15-5-73 from the Ural Branch of the Russian Academy of Sciences.

## REFERENCES

- Affi, A.M., Kelly, W.C., Essene, E.J., 1988a. Phase relations among tellurides, sulfides, and oxides: I. Thermodynamical data and calculated equilibria. *Econ. Geol.* 83, 377–394.
- Affi, A.M., Kelly, W.C., Essene, E.J., 1988b. Phase relations among tellurides, sulfides, and oxides: II. Application to telluride-bearing ore deposits. *Econ. Geol.* 83, 395–404.
- Andreev, A.V., Mansurov, R.Kh., 2008. The Novogodnenskoe gold field (Polar Urals), in: Proceedings of the Conference “Topical Problems of Geological Study of the Earth’s Interior and Restoration of the Solid Mineral Resources Base” [in Russian]. VIMS, Moscow, pp. 20–23.
- Augé, T., Salpeteur, I., Bailly, L., Mukherjee, M.M., Patra, R.N., 2002. Magmatic and hydrothermal platinum-group minerals and base-metal sulphides in the Baula Complex, India. *Can. Mineral.* 40, 277–309.
- Bai, L., Barnes, S.-J., Baker, D.R., 2017. Sperrylite saturation in magmatic sulfide melts: Implications for formation of PGE-bearing arsenides and sulfarsenides. *Am. Mineral.* 102 (5), 966–974.
- Bakker, R.J., 2014. Application of combined micro-Raman and electron probe microanalysis to identify platinum group minerals, in: 11th EMAS Regional Workshop on Electron Probe Microanalysis of Materials Today — Practical Aspects, September 2014, Leoben, Austria, pp. 215–233.
- Barkov, A.Y., Lafamme, J.H.G., Cabri, L.J., Martin, R.F., 2002. Platinum-group minerals from the Wellgreen Ni-Cu-PGE deposit, Yukon, Canada. *Can. Mineral.* 40, 651–669.
- Barnes, S.J., Fisher, L.A., Godel, B., Pearce, M.A., Maier, W.D., Pateron, D., Howard, D.L., Ryan, C.G., Laird, J.S., 2016. Primary cumulus platinum minerals in the Monts de Cristal Complex, Gabon: magmatic microenvironments inferred from high-resolution X-ray fluorescence microscopy. *Contrib. Mineral. Petrol.* 171 (3), 1285–1308.
- Borisenko, A.S., 1977. Study of the salt composition of solutions of gas–liquid inclusions in minerals by the cryometric method. *Geologiya i Geofizika (Soviet Geology and Geophysics)* 18 (8), 16–27 (11–19).
- Bortnikov, N.S., Cabri, L.J., Vikentiev, I.V., Tagirov, B.R., Mc Mahon, G., Bogdanov, Yu.A., Stavrova, O.O., 2003. Invisible gold in sulfides from seafloor massive sulfide edifices. *Geol. Ore Deposits* 45 (3), 201–212.
- Cabri, L.J., 1965. Phase relations in the Ag–Au–Te systems and their mineralogical significance. *Econ. Geol.* 60, 1569–1606.
- Cabri, L.J., 2002. The Geology, Geochemistry, Mineralogy and Mineral Beneficiation of Platinum-Group Elements. Canadian Institute of Mining, Metallurgy and Petroleum, Montréal, Spec. Vol. 54.
- Chang, Y.A., Goldberg, D., Neumann, J.P., 1977. Phase diagrams and thermodynamic properties of ternary gold–copper–silver systems. *J. Phys. Chem. Ref. Data* 6, 621–669.

- Chernyshov, N.M., Pereslavl'tsev, A.V., Kuznetsov, A.N., Kozlov, M.T., Kudryavtseva, O.A., 1990. Formation Types of Ultramafic–Mafic Intrusions of the Pai-Khoi Province and Their Nickel Potential [in Russian]. VGU, Voronezh.
- Ciobanu, C., Cook, N.J., Damian, G., Damian, F., Buia, G., 2004. Telluride and sulphosalt associations at acarimb, in: Cook, N.J., Ciobanu, C.L. (Eds.), *Gold–Silver–Telluride Deposits of the Golden Quadrilateral, South Apuseni Mts., Romania*. IAGOD Guidebook Series 12, 145–186.
- Cooke, D.R., Mc Phail, D.C., 2001. Epithermal Au–Ag–Te mineralization, Acupan, Baguio District, Philippines: numerical simulations of mineral deposition. *Econ. Geol.* 96, 109–131.
- Craig, J.R., Kullerud, G., 1969. Phase relations in the Cu–Fe–Ni–S system and their application to magmatic ore deposits. *Econ. Geol. Monogr.* 4, 344–358.
- Dare, S.A.S., Barnes, S.-J., Prichard, H.M., Fisher, P.C., 2010. The timing and formation of platinum-group minerals from the Creighton Ni–Cu–platinum-group element sulfide deposit, Sudbury, Canada: Early crystallization of PGE-rich sulfarsenides. *Econ. Geol.* 105, 1071–1096.
- Dare, S.A.S., Barnes, S.-J., Prichard, H.M., Fisher, P.C., 2011. Chalcophile and platinum-group element (PGE) concentrations in the sulfide minerals from the McCreey East deposit, Sudbury, Canada, and the origin of PGE in pyrite. *Miner. Deposita* 46 (4), 381–407.
- Evstigneeva, T., Tarkian, M., 1996. Synthesis of platinum-group minerals under hydrothermal conditions. *Eur. J. Mineral.* 8, 549–564.
- Faure, G., 1986. *Principles of Isotope Geology*. John Wiley & Sons, New York.
- Grinenko, V.A., 1962. Preparation of sulfur dioxide for isotope analysis. *Zhurnal Neorganicheskoi Khimii* 7, 2578–2582.
- Hanley, J.J., 2007. The role of arsenic-rich melts and mineral phases in the development of high-grade Pt–Pd mineralization within komatiite-associated magmatic Ni–Cu sulfide horizons at Dundonald Beach South, Abitibi subprovince, Ontario, Canada. *Econ. Geol.* 102, 305–317.
- Hannington, M.D., Scott, S.D., 1989. Sulphidation equilibria as guides to gold mineralization in volcanogenic massive sulfides: evidence from sulfide mineralogy and composition of sphalerite. *Econ. Geol.* 84 (7), 1978–1995.
- Helmy, H.M., Ballhaus, C., Fonseca, R.O.C., Wirth, R., Nagel, T.J., Tredoux, M., 2013. Noble metal nanoclusters and nanoparticles precede mineral formation in magmatic sulphide melts. *Nat. Commun.* 4, 2405, doi:10.1038/ncomms3405.
- Honea, R.M., 1964. Empressite and stuetzite redefined. *Am. Mineral.* 49, 325–338.
- Karakaya, I., Thompson, W.T., 1991. The Ag–Te (silver–tellurium) system. *J. Phase Equilib.* 12 (1), 56–63.
- Kim Won-Sa, Chao, G.Y., 1991. Phase relations in the system Pd–Sb–Te. *Can. Mineral.* 29, 401–409.
- Klyukin, Yu.I., 2012. The fluid regime of formation of gold–telluride mineralization of the Byn'govskoe deposit, Middle Urals. *Litosfera* 3, 127–138.
- Kovalenker, V.A., Zalibekyan, M.A., Laputina, I.P., Malov, V.S., Sandomirskaya, S.M., Garas'ko, M.I., Mkhitarian, D.V., 1990. Sulfide-telluride mineralization of the Megradzor ore field in Armenia. *Geologiya Rudnykh Mestorozhdenii* 3, 65–81.
- Kuznetsov, S.K., Maiorova, T.P., Shaybekov, R.I., Sokerina, N.V., Filippov, V.N., 2014. Mineral composition and formation conditions of gold–platinum–palladium ore occurrences in the northern Urals and Pai-Khoi, in: *Precious, Rare, and Radioactive Elements in Ore-Forming Systems* [in Russian]. INGG SO RAN, Novosibirsk, pp. 342–347.
- Lozhechkin, M.P., 1939. New data on the chemical composition of Cu-containing gold. *Dokl. Akad. Nauk SSSR* 24 (5), 454–457.
- Makovicky, E., 2002. Ternary and quaternary phase systems with PGE, in: Cabri, L.J. (Ed.), *The Geology, Geochemistry, Mineralogy and Mineral Beneficiation of Platinum-Group Elements*. Canadian Institute of Mining, Metallurgy and Petroleum, Spec. Vol. 54, 131–175.
- Mansurov, R.Kh., 2013. *Geological and Structural Conditions of Localization of the Petropavlovskoe Gold Deposit*. PhD Thesis [in Russian]. Moscow.
- Maslennikov, V.V., Maslennikova, S.P., Large, R.R., Danyush-evsky, L.V., Herrington, R.J., Stanley, C.J., 2013. Tellurium-bearing minerals in zoned sulphide chimneys from Cu–Zn massive sulphide deposits of the Urals, Russia. *Mineral. Petrol.* 107, 67–99.
- Mazzini, A., Svensen, H., Etiope, G., Onderdonk, N., Banks, D., 2011. Fluid origin, gas fluxes and plumbing system in the sediment-hosted Salton Sea Geothermal System (California, USA). *Volcanol. Geotherm. Res.* 205, 67–83.
- Murzin, V.V., Varlamov, D.A., 2018. Chemical composition of native gold in magnetite ores of the Kagan ultrabasic massif (South Urals), in: *Transactions of the Institute of Geology and Geochemistry of the Ural Branch of the Russian Academy of Sciences (Yearbook 2017)* [in Russian], Issue 165, 194–199.
- Murzin, V.V., Kudryavtsev, V.I., Berzon, R.O., Sustavov, S.G., 1987. Copper-containing gold in rodingitization zones. *Geologiya Rudnykh Mestorozhdenii* 29 (5), 96–99.
- Nikolaev, Yu.N., Prokof'ev, V.Yu., Apletalin, A.V., Vlasov, E.A., Baksheev, I.A., Kal'ko, I.A., Komarova, Ya.S., 2013. Gold–telluride mineralization of the western Chukchi Peninsula, Russia: mineralogy, geochemistry, and formation conditions. *Geol. Ore Deposits* 55 (2), 96–124.
- Oh, S.J., Cook, D.C., Townsend, H.E., 1998. Characterization of iron oxides commonly formed as corrosion products on steel. *Hyperfine Interact.* 112, 59–65.
- Ohmoto, H., Rye, R.O., 1979. *Isotopes of sulfur and carbon*, in: *Geochemistry of Hydrothermal Ore Deposits*. John Wiley & Sons, New York, pp. 509–567.
- Okamoto, H., Chakrabarti, D.J., Laughlin, D.E., Massalski, T.B., 1987. The Au–Cu (gold–copper) system. *Bull. Alloy Phase Diagrams* 8, 453–474.
- Ostashevchenko, B.A., 1979. *Petrology and Mineralization of the Central Pai-Khoi Basaltoid Complex* [in Russian]. Nauka, Leningrad.
- Pals, D.W., Spry, P.G., 2003. Telluride mineralogy of the low-sulfidation epithermal Emperor gold deposit, Vatukoula, Fiji. *Mineral. Petrol.* 79, 285–307.
- Petrovskaya, N.V., 1993. *Gold Nuggets* [in Russian]. Nauka, Moscow.
- Piña, R., Gervilla, F., Barnes, S.-J., Ortega, L., Lunar, R., 2012. Distribution of platinum-group and chalcophile elements in the Aguablanca Ni–Cu sulfide deposit (SW Spain): Evidence from a LA-ICP-MS study. *Chem. Geol.* 302–303, 61–75.
- Plotinskaya, O.Yu., Groznova, E.O., 2008. Formation conditions of the Berezhnyakovskoe epithermal Au–Ag–Te–Se deposit, South Urals, in: *Proceedings of the Thirteenth International Conference on Thermobarogeochemistry and the Fourth Symposium of APFIS* [in Russian]. IGEM, Moscow, Vol. 2, pp. 101–103.
- Plyusnina, L.P., Likhoidov, G.G., 2009. The behavior of platinum under hydrothermal conditions. *Vestnik DO RAN*, 4, 30–37.
- Plyusnina, L.P., Likhoidov, G.G., Shcheka, Zh.A., 2007. Experimental modeling of platinum behavior under hydrothermal conditions (300–500 °C) and 1 kbar. *Geochem. Int.* 45 (11), 1124–1130.
- Podosov, L.L. (Ed.), 2000. *State Geological Map of the Russian Federation. Scale 1:1,000,000 (New Series). Sheet R-(40)–42-o. Vaigach, Yamal Peninsula*. Explanatory Note [in Russian]. VSEGEI, St. Petersburg.
- Prokof'ev, V.Yu., Spiridonov, E.M., 2000. Composition of metamorphosed fluids and conditions of transformation of ores of the Kochkanarskoe gold deposit, in: *Proceedings of the Conference “Petrography on the Eve of the 21st Century: Results and Prospects”* [in Russian]. Syktyvkar, Vol. 3, pp. 88–90.
- Roizeman, F.M., 2008. *The Theory of Fluid Ore Formation under “Carbon Dioxide Wave” Impact* [in Russian]. MYU, Moscow.

- Shackleton, J.M., Spry, P.G., Bateman, R., 2003. Telluride mineralogy of the golden mile deposit, Kalgoorlie, Western Australia. *Can. Mineral.* 41, 1503–1524.
- Shaybekov, R.I., 2006. Dolerite body (Sopcha) of Central Pai-Khoi and its U–Pb (SHRIMP II) dating, in: The Third Siberian International Geoscience Conference of Young Scientists [in Russian]. OIGGM SO RAN, Novosibirsk, pp. 246–248.
- Shaybekov, R.I., 2013a. Gold–telluride mineralization in quartz–sulfide veinlets of the Krutoi ore occurrence (Pai-Khoi). *Vestnik IG Komi NTs UrO RAN*, No. 7, 13–16.
- Shaybekov, R.I., 2013b. Platinum–Sulfide Mineralization in the Pai-Khoi Gabbro-Dolerites [in Russian]. *Izd. Komi NTs UrO RAN, Syktyvkar*.
- Shaybekov, R.I., 2018. The first data on subburite mineral in Pai-Khoi, in: Recent Problems of Theoretical, Experimental, and Applied Mineralogy (Yushkin Readings 2018). Proceedings of Mineralogical Seminar with International Participants [in Russian]. IG Komi NTs UrO RAN, Syktyvkar.
- Shishkin, M.A., Shkarubo, S.I., Markina, N.M., Molchanova, E.V., Kalaus, S.V., 2009. The main results of the compilation of the complex state geological map on a scale of 1:1,000,000 (third generation), sheet R-41, in: Proceedings of the Conference “Geology and Mineral Resources of European Northeastern Russia” [in Russian]. IG Komi NTs UrO RAN, Syktyvkar, Vol. 2, pp. 183–185.
- Silaev, V.I., 1978. Mineralogy and Lithogenesis of Ordovician Deposits of Central Pai-Khoi [in Russian]. Nauka, Leningrad.
- Smirnov, S.Z., Bortnikov, N.S., Gonevchuk, G.N., Gorelikova, N.V., 2014. Melt compositions and fluid regime of crystallization of rare-metal granite and pegmatites from the Sn–W Tigrinoe deposit (Primor’e). *Dokl. Earth Sci.* 456 (1), 558–562.
- Sokerina, N.V., Shanina, S.N., Zykin, N.N., Isaenko, S.I., Piskunova, N.N., 2013. Conditions of formation of gold mineralization in the Sinil’ga ore occurrence, Subpolar Urals (from results of study of fluid inclusions). *Zapiski RMO*, No. 6, 89–105.
- Sokerina, N.V., Shaybekov, R.I., Shanina, S.N., Isaenko, S.I., 2016. The fluid regime of formation of gold–telluride–palladium mineralization in the Krutoi ore occurrence (Pai-Khoi). *Vestnik IG Komi NTs UrO RAN*, Issue 8, 9–13.
- Spiridonov, E.M., Gritsenko, Yu.D., 2009. Epigenetic Low-Grade Metamorphism and Co–Ni–Sb–As Mineralization in the Norilsk Ore Field [in Russian]. Nauchnyi Mir, Moscow.
- Spry, P.G., Scherbath, N.L., 2006. Vanadium silicates and oxides in the Tuvatu gold–silver telluride deposit, Fiji. *Mineral. Petrol.* 87, 171–176.
- Taylor, H.P., Jr., 1974. The application of oxygen and hydrogen isotope studies to problems of hydrothermal alteration and ore deposition. *Econ. Geol.* 69, 843–883.
- Ustritskii, V.I., 1954. Stratigraphy, Facies, and Tectonics of the Paleozoic Pai-Khoi Deposits [in Russian]. NIIGA, Leningrad.
- Vikentyev, I.V., 2006. Precious metal and telluride mineralogy of large volcanic-hosted massive sulfide deposits in the Urals. *Mineral. Petrol.* 87, 305–326.
- Voronin, M.V., Osadchii, E.G., Brichkina, E.A., 2017. Thermochemical properties of silver tellurides including empressite (AgTe) and phase diagrams for Ag–Te and Ag–Te–O. *Phys. Chem. Mineral.* 44, 639–653.
- Voudoris, P., 2006. A comparative mineralogical study of Te-rich magmatic-hydrothermal systems in northeast Greece. *Mineral. Petrol.* 87, 1438–1468.
- Watkinson, D.H., Melling, D.P., 1992. Hydrothermal origin of the platinum mineralization, Alaska. *Econ. Geol.* 87 (1), 175–184.
- Zaborin, O.V., 1975. Major Igneous Rocks of the Central Pai-Khoi Ridge (Yugor Peninsula). PhD Thesis [in Russian]. Leningrad.
- Zhai, D., Liu, J., 2014. Gold–telluride–sulfide association in the Sandaowanzi epithermal Au–Ag–Te deposit, NE China: implications for phase equilibrium and physicochemical conditions. *Mineral. Petrol.* 108, 853–871.
- Zykin, N.N., Sokerina, N.V., 2015. Genesis of waters of hydrothermal deposits in the Polar Urals. *Vestnik IG Komi NTs UrO RAN*, No. 9, 18–23.

*Editorial responsibility:* A.S. Borisenko